THE JOURNAL OF BIOLOGICAL CHEMISTRY VOL. 287, NO. 12, pp. 9147–9167, March 16, 2012


# Serine/Threonine Phosphatase (SP-STP), Secreted from *Streptococcus pyogenes*, Is a Pro-apoptotic Protein*[S]

Received for publication, October 22, 2011, and in revised form, December 30, 2011 Published, JBC Papers in Press, January 19, 2012, DOI 10.1074/jbc.M111.316554

**Shivani Agarwal**[1], **Shivangi Agarwal**[1], **Hong Jin, Preeti Pancholi, and Vijay Pancholi**[2]

*From the Department of Pathology, Ohio State University College of Medicine, Columbus, Ohio 43210-1214*

**Background:** Eukaryote-type serine/threonine phosphatase (SP-STP) of group A *Streptococcus* (GAS) is essential for virulence, but its direct role in causing pathological effects in the host remains unknown.
**Results:** SP-STP crosses two membrane barriers and causes apoptosis of human pharyngeal cells from within and without.
**Conclusion:** SP-STP is a quintessential virulence-controlling factor.
**Significance:** The study illustrates how GAS utilizes SP-STP to exploit host machinery for its own advantage.

**This investigation illustrates an important property of eukaryote-type serine/threonine phosphatase (SP-STP) of group A *Streptococcus* (GAS) in causing programmed cell death of human pharyngeal cells. The secretory nature of SP-STP, its elevated expression in the intracellular GAS, and the ability of wild-type GAS but not the GAS mutant devoid of SP-STP to cause apoptosis of the host cell both *in vitro* and *in vivo* suggest that GAS deploys SP-STP as an important virulence determinant to exploit host cell machinery for its own advantage during infection. The exogenously added SP-STP is able to enter the cytoplasm and subsequently traverses into the nucleus in a temporal fashion to cause apoptosis of the pharyngeal cells. The programmed cell death induced by SP-STP, which requires active transcription and *de novo* protein synthesis, is also caspase-dependent. Furthermore, the entry of SP-STP into the cytoplasm is dependent on its secondary structure as the catalytically inactive SP-STP with an altered structure is unable to internalize and cause apoptosis. The ectopically expressed wild-type SP-STP was found to be in the nucleus and conferred apoptosis of Detroit 562 pharyngeal cells. However, the catalytically inactive SP-STP was unable to cause apoptosis even when intracellularly expressed. The ability of SP-STP to activate pro-apoptotic signaling cascades both in the cytoplasm and in the nucleus resulted in mitochondrial dysfunctioning and perturbation in the phosphorylation status of histones in the nucleus. SP-STP thus not only functions as a virulence regulator but also as an important factor responsible for host-related pathogenesis.**

*Streptococcus pyogenes* (GAS),[3] despite being treatable by penicillin, remains the leading cause of a variety of diseases ranging from mild pharyngitis and superficial impetigo to debilitating toxic shock syndrome, necrotizing fasciitis, and autoimmune sequelae (1). GAS possesses complex gene regulatory networks to respond to subtle environmental changes and to thrive in the intricate and continuously fluctuating habitats in the human body and mucosal surfaces (2). Regulation of virulence factors and their temporal repertoire at a given site dictate the final outcome of the disease (3). Although GAS is predominantly recognized as an extracellular pathogen, it is now established that GAS invades host cells and persists intracellularly (4). In fact, GAS survives within phagocytes and macrophages and undergoes phenotypic switching resulting in a hypervirulent phenotype (5). The mechanism of this hypervirulence, which is likely due to a specific gene expression repertoire, is presently not known. Although the gene expression profiles of GAS adhered to human Detroit cells *in vitro* (6), and those associated with the pharynx in experimental primate models (3) have shown distinct gene expression profiles, the information on gene expression of the GAS population found within the human pharyngeal cells is presently lacking.

It is evident that many invading pathogens, including GAS, cause apoptosis in a variety of host cells, including human lung cells, neutrophils, macrophages, and keratinocytes (7–9). Although several reports demonstrating the ability of GAS to adhere to and invade human pharyngeal cells are available, the information on its ability to cause apoptosis of human pharyngeal cells is lacking. GAS has been shown to cause a significantly accelerated form of apoptosis with unique host gene expression profiles during interaction with human neutrophils (9). A multitude of cell-bound and secretory enzymes/virulence factors have been shown to contribute substantially to GAS pathogenesis (2). Specifically, nicotinamide adenine dinucleotide (NAD)-glycohydrolases in association with streptolysin-O (Slo) have been implicated in perturbing host cell behavior by conferring deleterious effects on the viability of the host (10). Slo has also been shown to induce apoptosis of human macrophage (11). Similarly, streptococcal pyrogenic toxin B/cysteine

* This work was supported, in whole or in part, by National Institutes of Health Grants AI64912 and AI76889 (to V. P.). This work was also supported by Ohio State University departmental funds (to P. P.).
[S] This article contains supplemental Tables S1–S4, Figs. S1–S6, and additional references.
[1] Both authors contributed equally to this work.
[2] To whom correspondence should be addressed: Dept. of Pathology, Ohio State University, 420 W. 12th Ave., TMRF-288A, Columbus, OH 43210-1214. Tel.: 614-688-8053; Fax: 614-688-3192; E-mail: Vijay.Pancholi@osumc.edu.
[3] The abbreviations used are: GAS, group A *Streptococcus* or *Streptococcus pyogenes*; SP-STP, *S. pyogenes* serine/threonine phosphatase; SP-STK, *S. pyogenes* serine/threonine kinase; STKK, kinase domain of SP-STK; MEM, minimal essential medium; MTT, 3-(4,5-dimethylthiazol-2-yl)-2,5-diphenyltetrazolium bromide; qRT, quantitative real time; Slo, streptolysin-O; CS, culture supernatant; CL, cell lysate; PI, propidium iodide; PARP, poly(ADP-ribose) polymerase.

protease (SpeB) has been shown to manifest apoptosis via activation of matrix metalloproteases resulting in TNF-$\alpha$ and sFasL activation (12). However, the information on the expression levels of the genes encoding for proteins that have been demonstrated to cause cytolysis/apoptosis in the intracellular GAS population found within pharyngeal cells is presently not available.

Thus, in this study, we first analyzed the ability of GAS to cause apoptosis of human pharyngeal cells and subsequently the gene expression profile of the GAS population found exclusively within the human pharyngeal cells following its invasion. In light of our recent investigations on the role of co-transcribing and cognately regulated SP-STK (SPy1625) (13) and SP-STP (SPy1626) (14) in GAS virulence, the gene expression analysis revealing SP-STP (*SPy1626*) as one of the highly expressed genes in the intracellular GAS population during its invasion of pharyngeal cells was intriguing. SP-STP, an anchorless protein, is found to be secreted by an unknown mechanism (13). It is highly conserved and belongs to a metal-dependent protein phosphatase (PP2C) family (15). Employing SP-STP knock-out GAS mutants, we recently demonstrated that SP-STP is not essential for GAS survival but is essential to maintain GAS virulence (14). The recent observation demonstrating the role of eukaryotic PP2C$\alpha$ and PP2C$\beta$ in promoting apoptosis of neuronal and endothelial cells (16) prompted us to hypothesize that the secreted SP-STP (13) can play a significant role in GAS-mediated apoptosis of pharyngeal cells from within and/or without. In this study, we have validated our hypothesis as follows: (i) by demonstrating the ability of SP-STP to cross cytoplasmic as well as nuclear membrane barriers to enter into the host nucleus and orchestrate signaling pathways that lead to programmed cell death in an *in vitro* tissue culture model of human pharyngeal cells, and (ii) by observing the presence and absence of apoptosis in the lungs of experimental septicemic mice infected with the wild-type and SP-STP knock-out GAS mutant strains, respectively.

## EXPERIMENTAL PROCEDURES

### Cell Lines and Bacterial Strains

The wild-type *S. pyogenes*, M1SF370 (ATCC 700294) and M1T15448 (17, 18), and their corresponding STP mutants and complemented strains were grown in Todd-Hewitt broth as described previously (14). *Escherichia coli* DH5$\alpha$ and BL21(pLysS) were grown in Luria-Bertani medium.

Detroit 562 (ATCC CCL-138, human pharyngeal carcinoma), A549 (ATCC CCL-185, lung carcinoma), and CAL 27 (ATCC CRL-2095, tongue squamous cell carcinoma) cell lines were grown and maintained in MEM with 10% FBS. The liver carcinoma epithelial cell line HepG2 (ATCC HB-8065) was grown and maintained in Eagle's minimum essential medium with 10% FBS at 37 °C and 5% $CO_2$.

### Transmission Electron Microscopy

For ultrastructural analysis, M1SF370-infected and SP-STP (0.5 $\mu$M)-treated and uninfected/untreated Detroit 562 cells ($1 \times 10^8$) were fixed in 2.5% glutaraldehyde and 4% paraformaldehyde in 0.1 M cacodylate buffer and processed at the Ohio State University central microscopy and imaging facility as described previously (19).

### TdT-mediated dUTP Nick End Labeling (TUNEL) Assay for GAS-mediated Apoptosis of Detroit 562 Pharyngeal Cells

DNA fragmentation in the pharyngeal cells treated with live and heat-killed wild-type M1SF370 GAS strain (multiplicity of infection of 100:1 bacteria/cell) was visualized by TUNEL reaction-based *in situ* cell death detection kit (Roche Diagnostics) as per the manufacturer's instructions. The wild-type GAS grown until mid-log phase ($A_{600} = 0.6$) was washed twice with 1× PBS (taken as live bacteria) followed by repeated (twice) incubation at 65 °C for 30 min and cooling at room temperature to obtain heat-killed GAS. The labeled cells treated with the indicated strains were visualized under a light microscope.

### Isolation of Internalized GAS from Detroit 562 Pharyngeal Cells and RNA Isolation

Confluent Detroit 562 cells were infected with the wild-type M1SF370 GAS at a multiplicity of infection of 100:1 bacteria/cell for 6 h. As a control, wild-type GAS was incubated with MEM alone (without pharyngeal cells) under identical growth and culture conditions. The nonadherent bacteria were removed, and the pharyngeal cells were subjected to trypsin/EDTA treatment and low speed ($100 \times g$ for 10 min at 4 °C) centrifugation. The resulting pellet constituting pharyngeal cells harboring the internalized GAS was lysed (1% Triton X-100, 50 units of DNase for 30 min at 37 °C) to release the internalized GAS in the supernatant after low speed centrifugation ($100 \times g$). The released internalized bacteria were harvested and washed by repeated high speed centrifugation at $16{,}000 \times g$ for 10 min at 4 °C. Total RNA was extracted from four independently obtained internalized (biological replicates) and four control noninternalized (without Detroit 562 cells) GAS populations using Qiagen RNeasy kit as described previously (19). The purity and integrity of the RNA were confirmed by Agilent 2100 Bioanalyzer (Agilent Technologies). cDNA from each of the total RNA samples was derived using reverse transcriptase and labeled with either AlexaFluor 555 or AlexaFluor 647 as described previously (19). Technical replicates in the form of dye-swap experiment were included for each biological replicates, and microarray slides were stained as described previously (19).

### Microarray Analysis and Quantitative Real Time PCR (qRT-PCR) for GAS

Oligonucleotide-based microarray analysis corresponding to the 1,769 open reading frames in the genome of *S. pyogenes* M1SF370 was performed as described previously (19). Data from eight experiments (four biological replicates each with its two technical replicates/dye swap) were submitted to Gene Expression Omnibus (GEO) repository (GSE27846). The results were statistically analyzed by on-line software "Comprehensive R- and Bioconductor-based web service for microarray data analysis" (CARMA-web) (20) as described before (19). The qRT-PCR was performed using Brilliant SYBR Green qPCR Master Mix (Roche Diagnostics) for the selected virulence genes using gene-specific primers (supplemental Table S1) in a

LightCycler®480 (Roche Diagnostics), and the results were analyzed using Exor4 software as described previously (19).

### Effect of Intracellular Environment on Expression and Release of SP-STP from GAS

To determine the effect of the intracellular environment on the release of SP-STP from GAS, we used a cell-free extract of Detroit 562 cells, an approach originally described to measure the motility of *Listeria monocytogenes* in *Xenopus* extract (21, 22). For this, Detroit 562 cells were infected with M1SF370 ($10^7$ CFUs) in the incomplete MEM for 6 h under standard conditions. The co-culture supernatant containing the nonadherent GAS was collected, and bacterium-free supernatant (NA-A-SS) was obtained by centrifugation. By incubating the same amount of GAS with MEM in the absence of Detroit cells, a parallel control supernatant was obtained (C-SS) in a similar way. For the cell extract control, the uninfected confluent culture was harvested after 6 h, and the lysate was centrifuged (20,000 × *g*) to obtain a clear supernatant as control cell lysate supernatant (C-CL-S). A similarly obtained 2 ml of duplicate crude cell lysate was incubated with $10^7$ CFUs of M1SF370 for 6 h under the same co-culture conditions as described above. The bacteria were centrifuged, and the clear supernatant was used to determine the expression level and amount of released SP-STP from GAS when incubated with the cell-free cytoplasmic content (I-SS). The CFUs of GAS in the initial inoculum and at the end of incubation were determined and found to be the same. Subsequently, proteins in all supernatants were TCA-precipitated and electrophoresed on SDS-PAGE followed by Western blotting and analyzed for the presence of SP-STP using affinity-purified rabbit anti-SP-STP polyclonal antibody (13).

### Fluorescence and Confocal Microscopy

Differential interference contrast images of the Detroit 562 cells ($1 \times 10^8$) treated with SP-STP (0.5 $\mu$M) for 24 h were obtained using a confocal microscope at the Ohio State University central microscopy and imaging facility. The SP-STP/EF-STP-treated Detroit 562 cells were subjected to Hoechst/PI staining and visualized under a fluorescence microscope. To determine the fate of SP-STP upon its interaction with Detroit 562 cells, AlexaFluor 488-labeled SP-STP (0.5 $\mu$M) was incubated with Detroit 562 cells, and its location within the cells was examined at 3, 6, 12, and 24 h. Hoechst33342 (blue) was used for staining the nucleus. The Z-stack images were captured for each time point in addition to the two-dimensional images.

### Construction and Purification of EF-STP and Catalytic Variants of SP-STP and Determination of Their Kinetic Properties

The catalytically inactive mutants of SP-STP were generated by the QuikChange site-directed mutagenesis kit (Agilent Technologies) using the wild-type SP-STP expressing plasmid pET14b-SP-STP (13) as a template and specific primers (supplemental Table S2). Using a similar strategy and primers specific for the gene *EF3121* encoding for EF-STP (supplemental Table S2), a structural homolog of SP-STP found in *Enterococcus faecalis*, recombinant $His_6$-tagged EF-STP, was produced (13). The recombinant $His_6$-tagged EF-STP, SP-STP, and the derived SP-STP mutated proteins (SP-STPD36A, SP-STPD192A, SP-STPD231A) were purified as described previously (13) followed by endotoxin removal using Detoxi-Gel™ (Pierce).

The serine/threonine phosphatase activity of the wild-type SP-STP, EF-STP, and catalytically inactive SP-STP proteins was carried out using *p*-nitrophenyl phosphate substrate-based colorimetric assay, and their $K_m$ and $V_{max}$ values were calculated as described previously (13). Furthermore, the ability of SP-STP and its point mutant, SP-STPD192A, to catalyze *in vitro* dephosphorylation of SP-STKK and the SP-STKK-phosphorylated substrate, myelin basic protein, was assessed in an *in vitro* phosphorylation assay as described previously (13).

### In Vitro Detection of Apoptosis

*In Vitro MTT-based Cell Viability Assay*—Detroit 562 cells were either untreated (control) or treated with the following: (*a*) increasing concentrations of wild-type SP-STP (0.05–1.0 $\mu$M); (*b*) EF-STP (0.05–1.0 $\mu$M); (*c*) 0.5 $\mu$M catalytic variants of SP-STP; and (*d*) wild-type GAS (M1SF370/M1T15448) and their respectively derived SP-STP knock-out mutants and complemented strains (14). Ten microliters of MTT (5 mg/ml) was added to each well in a final volume of 100 $\mu$l and incubated for 2 h. The insoluble purple-colored formazan crystals were extracted by acidified isopropyl alcohol (0.1 N HCl in isopropyl alcohol) containing 0.1% SDS, and the absorbance of the reduced MTT was measured spectrophotometrically at 570 nm.

*Effect of SP-STP Addition on Different Cell Lines*—The A549, CAL-27, and HepG2 cells were seeded at a density of $1 \times 10^8$ cells/well and incubated with varying concentrations of purified recombinant SP-STP (0.5, 1.0, and 2.0 $\mu$M) for 24 h, and the cell viability was evaluated using MTT assay as described above.

*Flow Cytometry*—Detroit 562 cells ($1 \times 10^8$) were treated with 0.1 and 0.2 $\mu$M of either SP-STP or EF-STP. The untreated cells were kept as control. Cells were stained with annexin-V-FITC and PI (10 $\mu$l) according to the manufacturer's instructions (BD Biosciences) and subjected to flow cytometric analysis (BD Biosciences, FACSCalibur). The changes in the fluorescence in the SP-STP-treated *versus* the control (untreated) cells were analyzed in the FL-1 and FL-2 quadrants corresponding to annexin-FITC and PI, respectively.

*Apoptosis Detection by Cell Death Enzyme-linked Immunosorbent Assay (ELISA)*—For ELISA, Detroit 562 and A549 cells, seeded in 96-well plates ($1 \times 10^8$ cells/well), were treated with 0.5 $\mu$M SP-STP for 24 h. The cytoplasmic fractions (CL) and culture supernatants (CS) were evaluated for apoptosis and necrosis, respectively, by using Cell Death Detection ELISA kit (Roche Diagnostics) according to the manufacturer's instructions. The absorbance obtained in the untreated cells was taken as control. The results were statistically analyzed from three independent experiments each performed in six replicate wells.

*JC-1-based Measurement of Mitochondrial Membrane Potential ($\Psi_m$)*—Detroit 562 cells ($1 \times 10^8$) treated with 0.5 $\mu$M SP-STP for 24 h were stained with JC-1 (Molecular Probes, 5 $\mu$g/ml), a cationic carbocyanine dye that accumulates in mitochondria and allows visual and differential measurement of the mitochondrial membrane potential. The experiment was performed as per the manufacturer's instructions followed by visu-

alization under a fluorescence microscope. The red (hyperpolarized, J-aggregates) and green (depolarized, monomer) fluorescence intensities were quantitated at an excitation/emission 485/580 and 485/530 nm, respectively (Fluostar Galaxy).

*Scratch-wound Assay*—The migration of Detroit 562 pharyngeal cells treated with SP-STP was assessed using a scratch wound assay. For this, prior to creating a linear wound using a sterile pipette tip, the confluent culture of Detroit 562 cell lines were either left untreated (control) or treated with SP-STP (0.5 $\mu$M) for 24 h at 37 °C. The impact of the SP-STP treatment on cellular proliferation and migration was microscopically monitored after 24 h.

### *In Vivo Detection of Apoptosis*

To investigate the role of SP-STP in the GAS-mediated apoptosis during *in vivo* infection, a group of five mice (CD-1, 6–7 weeks old, 22–24 g, Charles River Laboratories) was infected intravenously with 100 $\mu$l ($1 \times 10^7$ CFUs) or intranasally with 50 $\mu$l ($2 \times 10^8$ CFUs) of the wild-type and M1ΔSTP mutant GAS strains. The lungs from the infected mice were harvested 72 h post-infection, fixed, processed, and stained with hematoxylin and eosin (H&E) for histopathological analyses. The role of SP-STP in GAS-mediated apoptosis was analyzed by TUNEL assay to determine the extent of apoptosis in the infected lung tissues using ApopTag® peroxidase *in situ* apoptosis detection kit (Millipore S7100) as per the manufacturer's instructions, at Ohio State University Pathology Core Facility. All animal experiments were performed in accordance with the Ohio State University Institutional Animal Care and Use Committee (IACUC)-approved protocol as described previously (19).

### *STP-induced Cell Death in Presence of Specific Inhibitors*

Detroit 562 human pharyngeal cells were preincubated for 1 h with the following inhibitors: 1 $\mu$g/ml (3.55 $\mu$M) protein synthesis inhibitor cycloheximide (Sigma); 0.1 $\mu$g/ml (0.08 $\mu$M) transcription blocker actinomycin D (Sigma); 2 $\mu$M proteasome inhibitor MG132 (Biovision); 10 $\mu$M U0126 ERK1/2 inhibitor (Promega); 1 mM TNF-$\alpha$ inhibitor, TAPI-2 (Peptides International); 20 $\mu$M each of caspase-3 (benzyloxycarbonyl-DEVD-fluoromethyl ketone), caspase-9 (benzyloxycarbonyl-LEHD-fluoromethyl ketone), and general caspase (benzyloxycarbonyl-VAD-fluoromethyl ketone) inhibitors (Biovision). The treated cells were washed three times with 1× PBS and treated with 0.5 $\mu$M SP-STP for 24 h. The cell viability was then determined by MTT assay as described above. The control untreated cells as well as the cells treated only with inhibitors were used for data normalization.

### *Expression Levels of Apoptosis-related Markers by Immunoblot Analysis*

Cell lysates from SP-STP-treated Detroit 562 pharyngeal cells were probed with various antibodies, *viz.* Bcl-2, Fas, CAD, Bcl-xL, and BAD (Signal Transduction Laboratories); ERK1/2 and phospho-ERK1/2 (Santa Cruz Biotechnology); caspase-3 (catalog no. 9665), caspase-9 (catalog no. 9502), and PARP (catalog no. 9542) (Cell Signaling); and monoclonal hIL-8 (catalog no. MAB208) (R & D Systems). The blots were probed with secondary HRP-conjugated anti-rabbit/mouse antibodies (Amersham Biosciences) followed by chemiluminescence-based visualization of the immunoreactive signals.

### *Microarray and RT$^2$ Profiler$^{TM}$ PCR Array-based Expression Analysis of Apoptosis-related Genes in SP-STP-treated Detroit 562 Cells*

Total RNA was extracted from untreated (control) and SP-STP-treated (0.5 $\mu$M) pharyngeal cells for 6, 12, 24, and 36 h. The cDNAs generated in two biological replicates (6 h) were subjected to Affymetrix microarray (HG-U133_Plus2, 56,764 genes) and processed on Affymetrix robotic fluidic station at the Ohio State University Comprehensive Cancer Center Microarray Facility. The results were statistically analyzed by ArrayStar4 software (DNA Star).

For the SYBR Green-based pathway-specific qRT-PCR analysis (12, 24, and 36 h), custom designed apoptosis PCR array (PAHS-012) representing 84 different human apoptosis-related genes was used (SABiosciences). The qRT-PCR experiments were performed using three different biological samples (Roche Diagnostics 480) each in three replicates per gene. The results were analyzed employing Exor4 (Roche Diagnostics)/SABiosciences software, as per the manufacturer's instructions.

### *Quantitation of TNF-α Levels*

The TNF-$\alpha$ released in the culture supernatants of untreated (control) and SP-STP-treated (0.5 $\mu$M for 12, 24, and 36 h) pharyngeal cells was measured by BDOptEIA ELISA kit (BD Biosciences). The amount of TNF-$\alpha$ was quantitated based on the standard curve generated using known concentrations (2–500 pg/ml) of TNF-$\alpha$.

### *Detection of SP-STP in Different Subcellular Fractions of Detroit 562 Cells*

Detroit 562 cells ($1 \times 10^8$) treated with 0.5 $\mu$M SP-STP for 3, 6, 12, and 24 h were fractionated into cytoplasmic and nuclear fractions using the subcellular fractionation kit (Pierce) as per the manufacturer's instructions. The presence of SP-STP was detected by immunoblot analysis (13).

### *Circular Dichroism (CD) Spectroscopy*

Far-UV CD spectra of the recombinant wild-type SP-STP, SP-STPD192A, and EF-STP (3 $\mu$g/ml) were obtained using J-710 spectropolarimeter (Jasco Corp.). The spectra were acquired at 25 °C using a 10-mm cell and wavelengths between 200 and 240 nm, and with a scanning speed of 50 nm/min. The CD signals were converted to mean residual ellipticity (MRE) and were deconvoluted by K2d software (23). The tertiary structural changes in SP-STP and SP-STPD192A were also recorded in the near-UV range (250–300 nm).

### *Generation of FLAG-tagged stp/-stpD192A Fusion Constructs*

Plasmid p3×FLAG-CMV$^{TM}$-14 (pCMV-*FLAG*, Sigma) was used as the parental plasmid for expression of the wild-type SP-STP and its catalytic variant (SP-STPD192A) in fusion with FLAG epitope at the C terminus, employing gene-specific primers containing KpnI and BamHI sites (supplemental Table S2). The pCMV-*stp.FLAG* and pCMV-*stpD192A.FLAG* con-

structs were purified using endotoxin-free plasmid extraction kit (Qiagen) according to the manufacturer's instructions prior to transient transfections. The effect of the CMV promoter-driven expression of SP-STP and SP-STPD192A in pharyngeal cells ($1 \times 10^8$) was evaluated by transfecting pCMV-*FLAG*, pCMV-*stp.FLAG*, and pCMV-*stpD192A.FLAG* using Lipofectamine (Invitrogen). Both untreated and empty vector (pCMV-*FLAG*)-transfected pharyngeal cells were included as controls. The *in situ* expression of SP-STP-FLAG and SP-STPD192A-FLAG was investigated 72 h post-transfection by chemiluminescence-based immunoblot analysis employing anti-FLAG (Sigma) and anti-SP-STP polyclonal antibodies. The pharyngeal cells were allowed to express SP-STP-FLAG and SP-STPD192A-FLAG proteins for 36, 48, and 72 h and were subjected to MTT assay.

### Construction of SP-STP-GFP Chimera and Its Localization in Detroit 562 Cells

An in-frame fusion of the *stp* gene with the 3′-end of *gfp* was made employing pEGFP-C1 plasmid (Clontech) (supplemental Table S2) using primers containing KpnI and BamH1 sites as described above (supplemental Table S2). The resulting plasmid, pEGFP-STP, and the control plasmid, pEGFP-C1, were transfected in Detroit 562 cells ($1 \times 10^8$). The fusion protein GFP-STP was allowed to express for 12 and 24 h. The nuclear staining was done using Hoechst33342 and the samples were visualized under a Nikon fluorescence microscope.

### In Vitro Protein Kinase Assay and Analysis of Phosphorylation Status of Histones

The purified recombinant histone H1 (5 $\mu$g, New England Biolabs) was incubated either with CDK-1 (20 units, New England Biolabs) alone or with SP-STP (2 $\mu$g) in the presence of [$\gamma$-$^{32}$P]ATP as described previously (13). The samples were electrophoresed, autoradiographed, and Coomassie-stained. Western blotting of the same samples was carried out using anti-phospho-H1 antibody (Abcam).

The nuclear extracts harvested from untreated and SP-STP-treated (0.5 $\mu$M, 24 h) pharyngeal cells were Western-blotted and probed with anti-phospho-Ser$^{10}$-H3, anti-total H3 (Upstate Biotechnology, Inc.), anti-phospho-Thr$^{146}$-H1, and total anti-pan-H1 (Abcam) antibodies as described above.

## RESULTS

### Interaction of GAS with Human Pharyngeal Cells Results in Apoptosis

To determine the consequences of GAS interaction with human pharyngeal cells, Detroit 562 human pharyngeal cells were infected with M1SF370 and co-cultured over a period of 16 h, and the invasion profile was monitored at an interval of 1, 4, 8, and 16 h by electron microscopy. We observed progressive adherence by M1SF370 GAS leading to invasion of pharyngeal cells (Fig. 1*A*, *1 h* and *4 h*). After being surrounded by the intracellular phagolysosomal vacuoles and limited division, M1SF370 escaped from the vacuoles and was found free in the cytoplasm (Fig. 1*A*, *4 h*). On further incubation (8 and 16 h), the infected pharyngeal cells were found to undergo apoptosis showing typical nuclear condensation and shrunken cell size with externalized (or about to externalize) M1SF370 (Fig. 1*A*, *8 h* and *16 h*). Furthermore, only live and not the heat-killed wild type M1SF370 bacteria were able to cause nuclear fragmentation/condensation and apoptosis as revealed by the TUNEL assay (Fig. 1*B*). Because apoptotic cells were found to harbor intact GAS, and the heat-killed but adhering GAS were unable to cause apoptosis, we concluded that mere GAS adherence to pharyngeal cells was not sufficient to cause apoptosis but invasion of pharyngeal cells was a prerequisite.

Because the expression repertoire of several GAS secretory products, including those that have been shown to cause the host cell apoptosis, are growth phase-dependent (24, 25), we hypothesized that the GAS-mediated apoptosis of pharyngeal cells is likely growth phase-dependent. To determine this, we measured the ability of an equal number of M1SF370 harvested at early ($A_{600} = 0.4-0.5$), late ($A_{600} = 0.7-0.8$), and stationary growth ($A_{600} = 1-1.2$) to inhibit proliferation of pharyngeal cells by MTT assay. Our results showed that the early log phase grown M1SF370 was able to cause proliferation inhibition, *i.e.* apoptosis in almost 90% pharyngeal cells as against 0–30% inhibition by the stationary and late log phase cultures (Fig. 1*C*). These results suggested that GAS grown at early to mid log phase has maximal capacity to invade, and the proteins expressed and secreted during this growth phase are likely playing a key role in causing apoptosis of pharyngeal cells. These results and the previously published report demonstrating increased virulence of intracellular GAS found within professional phagocytes (5) prompted us to determine global gene expression profiles of early to mid-log phase grown GAS exposed to the intracellular environment of human pharyngeal cells and to investigate the changes in the virulence potential of the intracellular GAS.

### GAS Exposed to Intracellular Environment Displays Significantly Elevated Levels of Virulence-related Genes, Including SP-STP

The evaluation of the total eight microarray-based global gene expression profiles of the invaded GAS population obtained after co-culturing Detroit 562 pharyngeal cells with mid-log phase-grown M1SF370 *versus* GAS not in contact with Detroit pharyngeal cells (for 6 h) revealed a total of 432 significantly differentiated genes (supplemental Tables S3 and S4). Although most of the genes (349/432 *i.e.* 80.8%) were up-regulated, 83 genes were down-regulated contributing to 19.2% of the total differentiated genes (supplemental Tables S3 and S4). Notably, the up-regulated genes belonged to amino acid and carbohydrate transport and metabolism, cell division and cell envelope biogenesis, DNA replication, and GAS virulence (supplemental Tables S3 and S4). Almost one-fourth of the differentially expressed genes (106/432) belonged to a category of unknown or possible predicted functions.

Further microarray analysis for the invaded GAS population indicated that 12/15 virulence-related genes were found to be highly up-regulated (supplemental Tables S3 and S4). In addition, several genes responsible for the regulation of GAS virulence, including those encoding for eukaryote-type Ser/Thr kinase (SPy1625/SP-STK, 2.5-fold) and Ser/Thr phosphatase

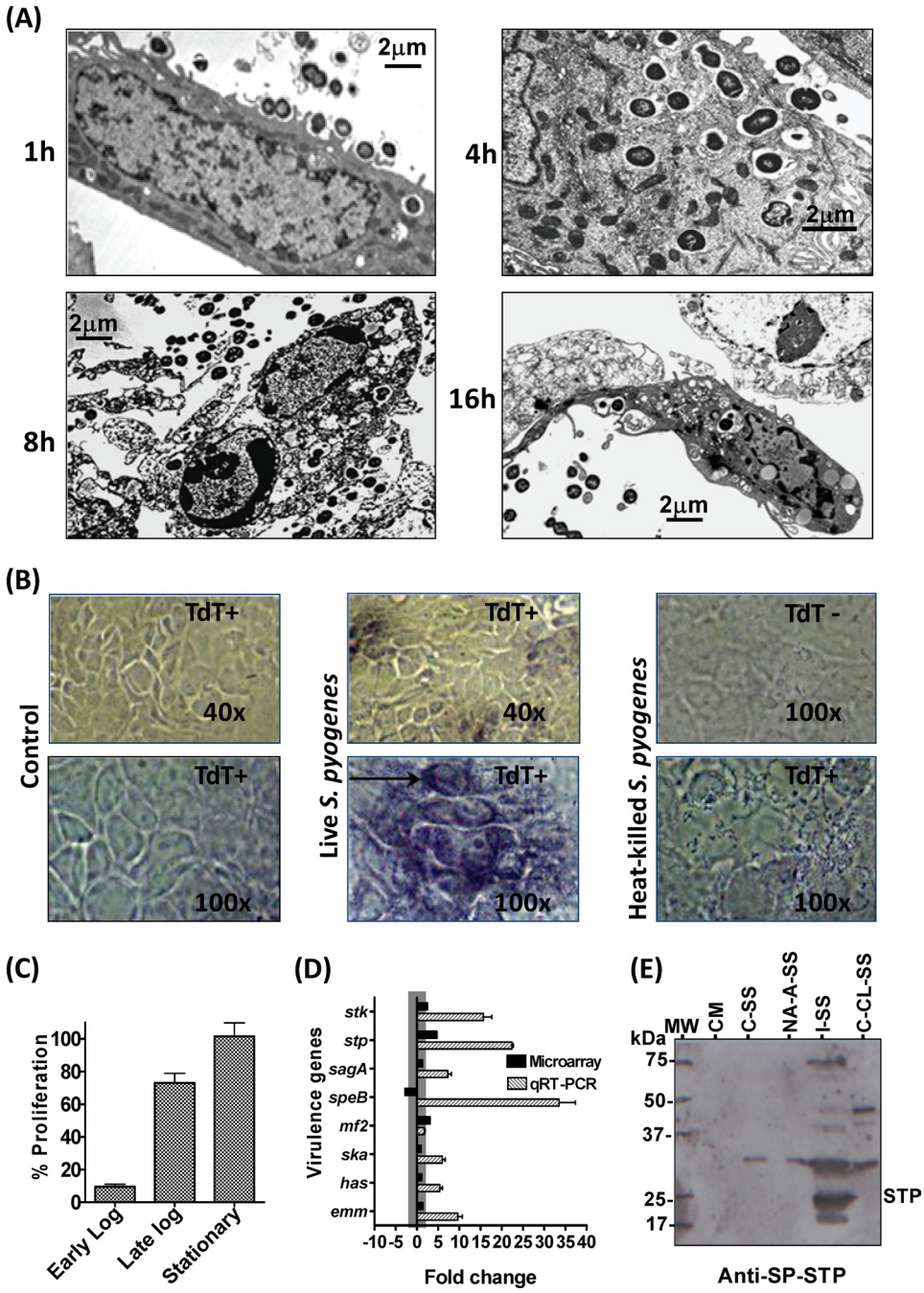


FIGURE 1. **Role of SP-STP in GAS-mediated apoptosis.** *A,* transmission electron microscopy of Detroit 562 cells infected and co-cultured with mid-log phase grown M1SF370 for different incubation times as indicated. *Scale bars* show indicated measurement. *B*, TUNEL assay (DNA fragmentation) demonstrating the ability of M1SF370 GAS (live *versus* heat-killed) to cause apoptosis of Detroit 562 cells. *C*, MTT assay-based determination of percentage proliferation of Detroit 562 cells in the presence of early log, late log, and stationary phase grown M1SF370. The % proliferation inhibition was calculated by considering proliferation of untreated cells as 100%. *D,* comparison of the expression levels of selected virulence-related genes by microarray and qRT-PCR analyses for M1SF370 GAS population found exclusively within Detroit 562 human pharyngeal cells. *E,* comparison of the influence of extracellular environment and intracellular content of Detroit 562 cells on the ability of GAS to express and secrete SP-STP. Western blot analysis of the TCA-precipitated samples (Samples 1–5) obtained as described under "Experimental Procedures" and probed with anti-SP-STP antibody. The migration of molecular weight marker is shown as *MW*; *1st lane,* CM-Tissue culture medium control; *2nd lane,* C-SS-GAS in MEM without Detroit 562 cells; *3rd lane,* NA-A-SS-Co-culture supernatant containing nonadherent GAS and secreted products of adherent GAS; *4th lane,* I-SS-GAS incubated with cell-free extract (whole cell lysate of Detroit 562 cells); and *5th lane,* C-CL-SS-control cell lysate obtained from cultured Detroit 562 cells incubated without GAS.

(SPy1626/SP-STP, 4.7-fold) (13,14, 19, 26), were also found to be up-regulated (Fig. 1*D* and supplemental Tables S3 and S4). Further validation of the mRNA expression profile of the eight major virulence-related genes by qRT-PCR assay (Fig. 1*D*) revealed up-regulation of genes encoding SPy2039/SpeB, SPy2018/Emm1, SPy1625/SP-STK, SPy1626/SP-STP, SPy0711/Mf2, SPy2200/HasA, SPy1979/Ska, and SPy0738/SagA by 2–30-fold. This expression profile suggested that the proteins encoded by these genes might contribute significantly to the increased virulence potential of GAS upon its invasion in the pharyngeal cells and likely gets accumulated within the cytoplasm.

In light of the above results revealing a 5-fold increase in the *stp*-specific transcript and secretory nature of SP-STP (13), we hypothesized that during GAS infection and upon its invasion of pharyngeal cells, GAS responds to a unique intracellular environment, and SP-STP is overexpressed, secreted, and eventually accumulated within the pharyngeal cells. However, based on our previous experiments (13), we have observed that only about 15–20% of the initial inoculum associates with the host cells, and only 2–5% of this associated population invades the host cells (13, 14, 19, 27, 28). Thus, to determine the amount of SP-STP released from the same number of nonadherent or adherent (exposed to extracellular environment) *versus* the invaded GAS population (exposed to the intracellular environment), we separately incubated an equal number of GAS to the intact Detroit cells and to the cell-free extract obtained from the same number of Detroit cells. The presence of SP-STP as determined by immunoblot analysis revealed the presence of SP-STP (27-kDa protein) only in the I-SS (Fig. 1*E*, *5th lane*, supernatant of GAS incubated with the cell-free extract) but not in the CM (Fig. 1*E*, *2nd lane, control medium*), C-SS (Fig. 1*E*, *3rd lane*, GAS supernatant incubated in MEM without Detroit cells), NA-A-SS (Fig. 1*E*, *4th lane*, co-culture medium containing nonadherent bacteria and released product from the adherent bacteria), and CL-S (Fig. 1*E*, *6th lane,* only cells). Because SP-STP possesses sequence similarity with the eukaryotic PP2C (hence called eukaryote-type STP (13, 26)), we attributed the non-SP-STP reactivity with high molecular weight protein bands to the cross-reacting proteins of Detroit cells and/or MEM used in this study. In conjunction with these results, microarray and qRT-PCR analysis laid the basis to determine fate of the following: 1) SP-STP secreted from GAS (from without), and 2) intracellularly accumulated SP-STP (from within), and overall impact of this spatiotemporal forms of SP-STP in the GAS-mediated apoptosis of pharyngeal cells.

### SP-STP Contributes Significantly to the GAS-mediated Apoptosis

Along with the above results and based on the recent reports implicating the role of the PP2C family of phosphatases in mediating neuronal cell death (apoptosis) (16, 29), we hypothesized that the extracellularly released (Fig. 1*C*) (13) and intracellularly accumulated SP-STP (Fig. 1, *D* and *E*) is likely to perform the classical PP2C-type apoptotic functions in pharyngeal cells from without and within.

Because we were able to successfully derive SP-STP knockout mutants from two type M1 GAS strains, M1SF370 and M1T15448 (14), we employed them as a tool to decipher the specific role of SP-STP in GAS-mediated apoptosis. The results from the MTT assays revealed significantly lower inhibition of proliferation of pharyngeal cells treated with GAS strains devoid of SP-STP (M1ΔSTP and M1T1ΔSTP, 5 and 18%, respectively) unlike the wild-type GAS strains (>90% inhibition) (Fig. 2*A*). The restoration of proliferation inhibition in the *stp*-complemented mutant strains (M1ΔSTP::*stp*->90%; M1T1ΔSTP::*stp*-72%) confirmed that SP-STP plays a significant role in GAS-mediated apoptosis (Fig. 2*A*). Because SP-STP is essential for the maintenance of GAS virulence and is not required for GAS survival (14), these results indicate that the ability of GAS to cause apoptosis is an important attribute of its virulence and pathogenesis.

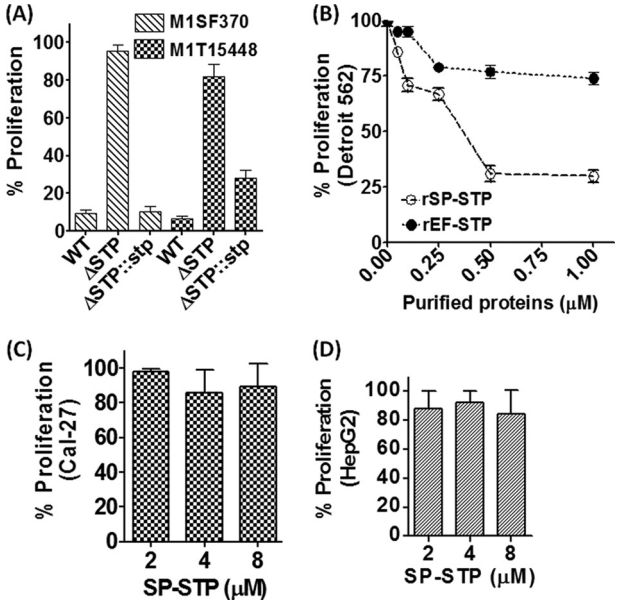


FIGURE 2. **Cell type-specific role of SP-STP in mediating apoptosis.** *A,* comparison of the ability of the wild-type (M1SF370 and M1T15448), isogenic nonpolar SP-STP-knock-out mutants (M1ΔSTP and M1T1ΔSTP), and the STP mutants complemented with the *stp* gene (M1ΔSTP::*stp* and M1T1ΔSTP::*stp*) (14) to inhibit proliferation of Detroit 562 cells infected at a multiplicity of infection of 100:1 (GAS CFUs:Detroit 562 cells) as revealed by MTT assay. *B,* MTT assay demonstrating the dose-dependent effect of the purified recombinant SP-STP and EF-STP on the proliferation of pharyngeal cells. MTT assay demonstrating the dose-dependent effect of the purified recombinant SP-STP on the proliferation of Cal-27 (*C*) and HepG2 cells (*D*).

The secretory nature SP-STP (13) led us to envision that during the interaction of GAS with the host cells, the secreted SP-STP from adherent bacteria may directly interact with the host cells. To understand the implications of this direct interaction and specificity, we first observed the ability of Detroit 562 cells to proliferate in the presence of increasing concentrations (0.05–1.5 μM) of purified SP-STP, and its structural homolog EF-STP. Although both purified SP-STP and EF-STP (see supplemental Fig. S1) are enzymatically active with comparable phosphatase activities (EF-STP $K_m$ = 0.125 mM; SP-STP $K_m$ = 0.35 mM) (13), only SP-STP and not EF-STP displayed dose-dependent proliferation inhibition of Detroit pharyngeal cells (Fig. 2*B*). Furthermore, SP-STP even at higher concentrations (2.0–8.0 μM) displayed no effect on the proliferation of Cal-27 and HepG2 cells (Fig. 2, *C* and *D*) indicating that the interaction of SP-STP with the cell type and subsequently its ability to cause apoptosis is cell type-specific.

### SP-STP Mediates Apoptosis and Not Necrosis of Human Respiratory Cells

To investigate whether the specificity of SP-STP to cause apoptosis is human respiratory cell type-specific, we evaluated the effect of SP-STP on human lung carcinoma cell line (A549). The latter was found to be as susceptible as Detroit 562 cells and showed 75% proliferation inhibition (apoptosis) when incubated with SP-STP (Fig. 3*A*). To further confirm that SP-STP-mediated proliferation inhibition in these two cell lines is due to apoptosis and not necrosis, we measured the presence of

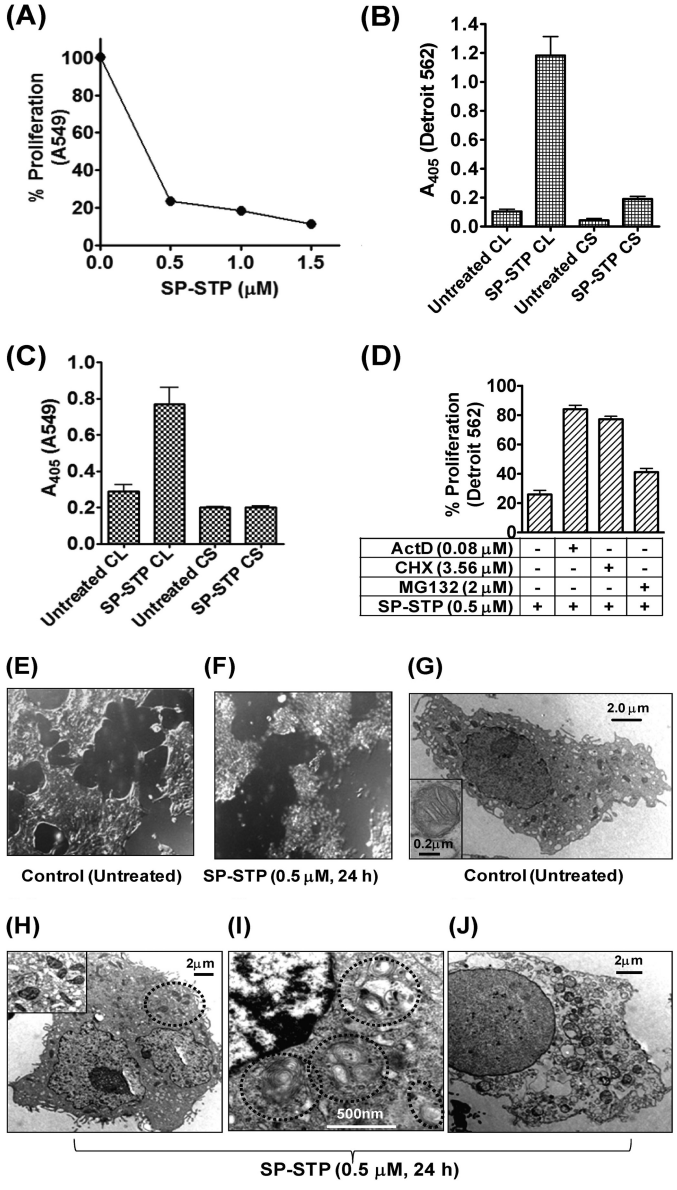


FIGURE 3. **SP-STP-mediates apoptosis and not necrosis of human respiratory cells.** *A,* MTT assay demonstrating the dose-dependent effect of the purified recombinant SP-STP on the proliferation of A549. *B* and *C,* absorbance (405 nm)-based cell-death detection assay depicting the presence or absence of nucleosomal fragments in the culture supernatant (*CS*) and corresponding cell lysates (*CL*) of Detroit 562 (*B*) and A549 cells (*C*) to monitor the extent of necrosis and apoptosis in SP-STP-treated cells. *D,* MTT assay demonstrating the effect of transcription inhibitor actinomycin D (*ActD*), protein synthesis inhibitor cycloheximide (*CHX*), and proteasome inhibitor (*MG132*) on SP-STP-mediated proliferation inhibition of Detroit 562 cells. The proliferation of cells treated with the inhibitors alone in each case was taken as control. *E* and *F,* differential interference contrast images obtained by light microscopic analysis of pharyngeal cells upon SP-STP (0.5 μM, 24 h) treatment. Ultrastructural analysis of untreated (*G*) and SP-STP-treated (*H–J*) Detroit 562 cells. Apoptotic Detroit 562 cells showing: *H,* severely damaged mitochondria; *I,* nuclear indentations, prominent autophagic membranes/vacuoles (*dotted circles*), and incipient chromatin condensation. *J,* late-stage apoptotic cell with loss of cellular organelles. *Scale bars* show indicated measurement.

nuclear contents in the SP-STP-treated culture supernatant (CS) and the corresponding cell lysate (CL). The lack of absorbance in the CS fraction unlike the CL fraction of the SP-STP-treated Detroit 562 (Fig. 3*B*) and A549 cells (Fig. 3*C*) revealed the absence of any oligonucleosomes/DNA fragments indicating that the observed proliferation inhibition (Figs. 2*B* and 3*A*) was not due to the toxic effect of SP-STP leading to the rupture of plasma and nuclear membranes, a typical characteristic feature of necrosis.

Because the human pharynx is the major and primary site of GAS infection, we primarily focused on the Detroit 562 cells in subsequent experiments. We observed that the SP-STP-mediated proliferation inhibition was abrogated in the presence of actinomycin D and cycloheximide (~80 *versus* 25% proliferation, Fig. 3*D*) indicating that the interaction of SP-STP with the pharyngeal cells results in the apoptotic signaling cascade wherein the cellular transcriptional and translational machineries play a key role. Additionally, the observed partial abrogation of proliferation inhibition (42% *versus* 25%, Fig. 3*D*) in SP-STP-treated Detroit 562 cells in the presence of proteosome inhibitor MG132 suggested the involvement of proteosomal machinery to some extent in facilitating SP-STP-mediated cell death. Together, these results indicate that SP-STP-mediated proliferation inhibition is not due to necrosis but rather is manifested by coordinated and regulated active transcription and translation of apoptosis-inducing proteins and protein degradation.

To further investigate cellular intactness of and other cellular changes in Detroit 562 cells subsequent to SP-STP treatment, the cells were monitored by light and transmission electron microscopy. Light microscopy of the SP-STP-treated cells displayed distinct rounding of the cells that were loosely attached to the surface of the tissue culture flasks, indicative of cells undergoing apoptosis (Fig. 3, *E* and *F*). The electron microscopic evaluation of the SP-STP-treated pharyngeal cells revealed the typical features of cell undergoing apoptosis. More specifically, SP-STP-treated cells displayed shrunken morphology with enlarged, convoluted, and multiple nuclei (Fig. 3, *G versus H*). The nuclei also displayed fragmented and condensed chromatin at the nuclear membrane/pole (Fig. 3*I*). Compared with the untreated control cells (Fig. 3*G*), the cytoplasm of SP-STP-treated cells displayed significantly fewer mitochondria, most of which were found to be either swollen with distorted shape or broken cristae (Fig. 3*H*, see *inset*). The observed irregularities in the cell shape upon SP-STP treatment in conjunction with membrane blebbing and the appearance of prominent autophagic membranes (Fig. 3*I*, *within dotted circles*) indicated that the binding of SP-STP to Detroit 562 cells indeed evokes a programmed cell death pathway. Certain cells were also found to be devoid of all the intact cytoplasmic organelles but increased vacuolar contents, indicating the onset of the later stages of apoptosis (Fig. 3*J*). The intact nature of both nuclear and plasma membranes in the late-stage apoptotic cells further substantiated the apoptotic nature of cell death induced by SP-STP.

### *Biochemical Evidence of SP-STP-mediated Apoptosis of Detroit 562 Cells*

Flow cytometric analysis of the annexin-V-FITC-stained SP-STP/EF-STP-treated (0.1 and 0.2 μM) and untreated pharyngeal cells revealed incorporation of the stain in 37% of the SP-STP-treated cells in comparison with the control (untreated) cells. However, EF-STP-treated cells did not show any detectable fluorescence signal indicating that the apoptosis conferred

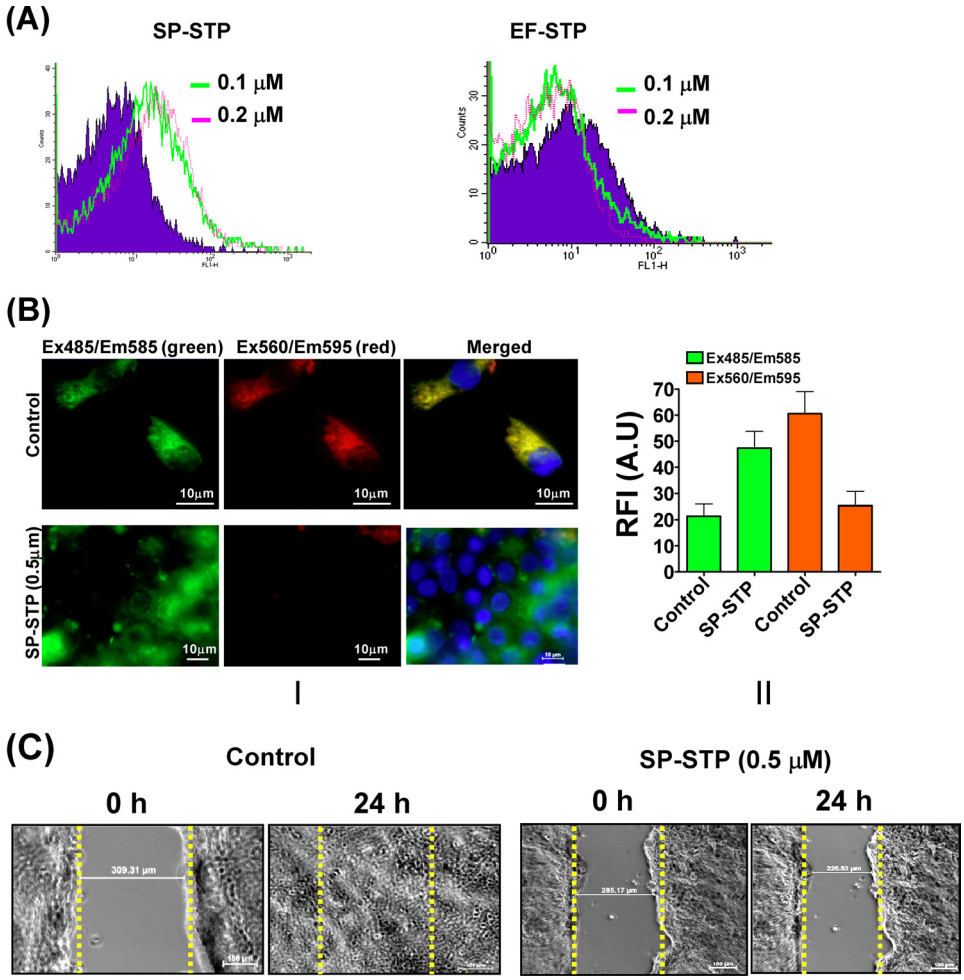


FIGURE 4. **Biochemical basis of SP-STP-mediated apoptosis of Detroit 562 cells.** *A,* flow cytometric analysis of the annexin-V-FITC-stained SP-STP and EF-STP treated (at indicated concentrations) pharyngeal cells. Ten thousand events were counted, and the shift in the FL-1 quadrant in comparison with the untreated cells was taken as reference to calculate percentage of apoptotic cells. *B,* effect of SP-STP treatment on the mitochondrial membrane potential ($\Psi_m$). *Panel I, upper row* shows JC-1-stained control cells showing *green*, *red orange*, and merged *yellow* fluorescent aggregates. The *lower panel* shows SP-STP-treated cells showing diffused *green* fluorescence dispersed throughout the cytoplasm with minimal *red orange* fluorescent aggregates. *Panel II,* quantitative assessment as measured by the ratio of *red versus green* (hyperpolarized *versus* depolarized) fluorescence in the untreated *versus* the SP-STP-treated (0.5 μM, 24 h) pharyngeal cells. *A.U.*, arbitrary units. *C, in vitro* wound healing scratch assay showing the extent of cell migration and closing of the wound (distance in micrometers in untreated (*control*) and SP-STP treated (0.5 μM, 24 h) pharyngeal cells within 24 h.

by SP-STP on human pharyngeal cells is specific (Fig. 4*A*). Similar results were obtained when SP-STP-treated (0.5 and 1.0 μM) Detroit 562 cells were stained with the Hoechst33342/PI. Brightly stained Hoechst-positive apoptotic nuclei with distinct chromatin fragmentation and condensation were observed in 30–40% of the cells treated with SP-STP (supplemental Fig. S2). The staining patterns of EF-STP-treated and untreated pharyngeal cells (control) were identical, supporting the fact that EF-STP does not cause apoptosis.

Ultrastructural analysis of SP-STP-treated pharyngeal cells revealing swelling and distortion in the mitochondria (Fig. 3*H*) prompted us to evaluate the perturbation in the mitochondrial membrane potential, a hallmark of cells undergoing apoptosis. This was determined by exploiting a lipophilic cationic potentiometric dye, JC-1, which forms red aggregates in the mitochondria of live cells possessing higher membrane potential ($\Psi_m$) (Fig. 4*B*, *panel I*). The SP-STP-treated cells displayed diffused green fluorescence dispersed throughout the cytoplasm indicating disrupted $\Psi_m$ (Fig. 4*B*, *panel I*). Unlike the distinct red/orange fluorescent aggregates (decreased green/red fluorescence ratio) observed in healthy cells, the pharyngeal cells treated with SP-STP showed increased green/red fluorescence ratio, further confirming mitochondrial membrane depolarization and dysfunctioning (Fig. 4*B*, *panel II*).

In support of other assays described above, we also performed the *in vitro* wound healing scratch assay. In this assay, the control Detroit pharyngeal cells were able to proliferate and migrate normally from the edge of the scratch and enclose the generated wound within 24 h (149.30 μm at $T_{0\,h}$ to 0 μm at $T_{24\,h}$) (Fig. 4*C*). The cells treated with SP-STP (0.5 μM for 24 h), however, did not show significant proliferation or migration after 24 h (226.35 μm at $T_{0\,h}$ to 215.25 μm at $T_{24\,h}$). These results indicated that SP-STP confers anti-proliferative effects and inhibits migration of Detroit 562 human pharyngeal cells.

### *SP-STP Plays a Significant Role in GAS-mediated Apoptosis in Vivo Experimental Septicemia and Lung Infection*

Based on our recent report demonstrating the essential role of SP-STP in GAS virulence and pathogenesis (14), we intended to establish a physiological link between the pro-apoptotic

nature of SP-STP and its role in the regulation of GAS virulence in *in vivo*. To this end, mice were infected intravenously and intranasally to develop systemic and lung infections. Because in mouse the pharynx is not anatomically differentiated, we measured the extent of infection and the apoptosis in lung tissues. Lungs from mice infected with wild-type M1SF370 displayed highly inflamed and constricted alveoli with inflammatory exudates within alveolar space as compared with lungs from mice infected with M1ΔSTP (Fig. 5*A*). In the TUNEL assay, a significant number of TUNEL-positive cells were found in the lungs of wild-type M1SF370-infected mice as compared with the lungs of M1ΔSTP-infected mice (average 60 *versus* 3 cells/field in septicemia and 15 *versus* 3 in intranasal infection model, $p < 0.001$) (Fig. 4*B*). These results clearly indicated that SP-STP-mediated apoptosis plays a significant role in GAS-mediated apoptosis and pathogenesis.

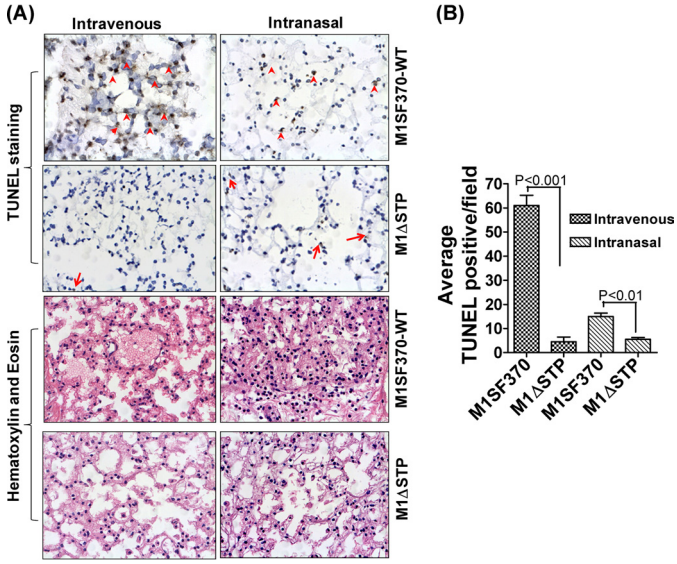


FIGURE 5. **TUNEL assay and histopathology of lungs of mice infected with wild-type (M1SF370) and isogenic mutant (M1ΔSTP) GAS strains.** *A,* TUNEL and H&E staining of lungs of mice infected (intravenous or intranasal) with M1SF370 or M1ΔSTP (*red arrows/arrowheads*) show representative TUNEL-positive alveolar cells in *brown*. *B,* average TUNEL-positive cells per field obtained from three independent tissue sections.

### *SP-STP Crosses Two Membrane Barriers and Enters into the Nucleus of Pharyngeal Cells*

Because SP-STP-treated Detroit 562 cells undergo apoptosis, we hypothesized that the apoptosis either occurs from without by direct binding of SP-STP to its putative receptor on the cell surface or from within as SP-STP subsequently migrates to the cytoplasm. For this, we monitored the fate of AlexaFluor488-labeled SP-STP at an early time point (3 h) that revealed that the SP-STP did enter the cells, but the majority of the fluorescence-labeled SP-STP was accumulated near the cell membrane. Following 6 h of incubation, the labeled SP-STP was found to be uniformly distributed within the cytoplasm (more than 40% the cells), and some amount was also localized peripheral to the nuclear membrane (Fig. 6*A*). The Z-stack images obtained at the 12 and 24 h of incubation revealed the superimposition of the green signal (AlexaFluor488-labeled STP) with the brightly stained red nuclei, generating a merged yellow fluorescence. Also, the red and green signals disappeared alternatively upon changing the fields in three dimensions indicating a progressive transmigration of the protein toward the nucleus. More than 70% of the total cells displayed the labeled SP-STP within the nucleus. These cells were also found to be rounded off with distorted nuclei and fragmented chromatin (Fig. 6*A*).

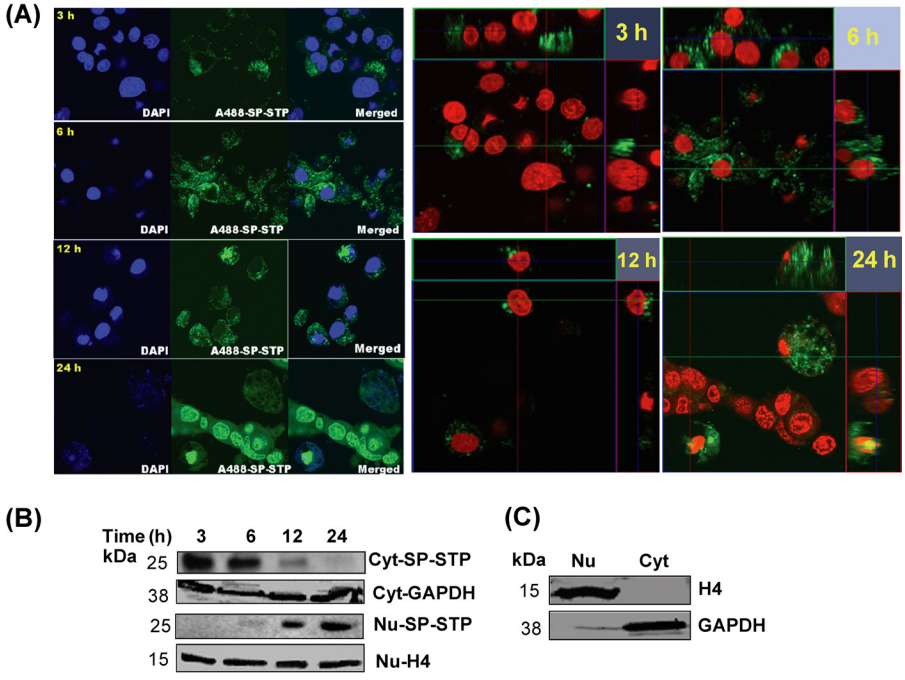


FIGURE 6. *A,* temporal migration of AlexaFluor488-SP-STP in pharyngeal cells over a period of 24 h. The two-dimensional and the Z-stack images depict the migration of SP-STP. Nucleus is stained with Hoechst33342. The *blue channel* was changed to *red* for showing the merged fluorescence (*yellow*) in the Z-stacks. *B,* Western immunoblots showing temporal migration of SP-STP from cytoplasmic (*Cyt*) to nuclear (*Nu*) compartments as revealed by anti-SP-STP antibody. *C,* cytoplasmic GAPDH and nuclear histone H4 are shown as loading and purity controls.

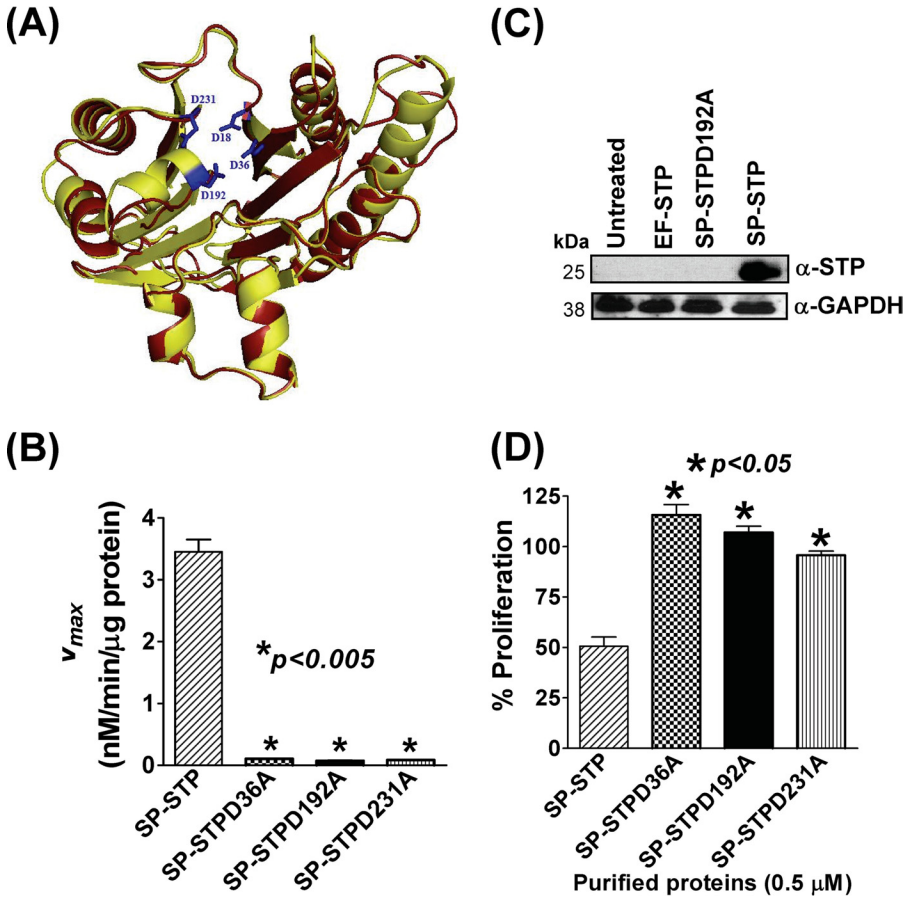


FIGURE 7. *A,* superimposed three-dimensionally derived structures of SP-STP (*yellow,* active site residues highlighted in *blue*) and EF-STP (*red*) based on *S. agalactiae* STP (30) (Protein Data Bank code 2PK0; MMDB code 46589). *B,* kinetic analysis showing the catalytic coefficients ($V_{max}$ in μM/min/μg protein) of the wild-type SP-STP and its mutant proteins. *C,* Western blot analysis of the cell lysates harvested from SP-STP-, SP-STPD192A-, and EF-STP-treated pharyngeal cells and probed with anti-SP-STP antibody revealing the ability of the purified proteins to internalize the pharyngeal cells. Cell lysate prepared from untreated pharyngeal cells was taken as control, and GAPDH was used as loading control. Cell fractionation was carried out as in Fig. 6*B*. *D,* MTT assay showing the effect of wild-type SP-STP and the catalytically inactive mutant proteins on proliferation of Detroit 562 cells.

The observed ability of the SP-STP to internalize pharyngeal cell membrane and progressively migrate to the nuclear membrane and subsequently enter into the nucleus was further confirmed by fractionating the cytoplasmic and nuclear fractions of cells treated with SP-STP. The results clearly indicated a significant reduction in the amount of SP-STP in the cytoplasmic fraction from 12 to 24 h. The SP-STP was found to accumulate maximally in the nucleus after 24 h of incubation (Fig. 6*B*). Together, these results showed the unique property of SP-STP to penetrate two membrane barriers and enter into the nucleus.

### *Internalization of SP-STP in Detroit 562 Cells Is Linked to Its Phosphatase Activity*

Because SP-STP binds, internalizes, and migrates through cytoplasm to the nucleus of the pharyngeal cells, we explored whether its structure, which is maintained by the catalytic domain responsible for its phosphatase activity, plays any role in binding and hence its internalization into the pharyngeal cells and subsequent activation of apoptosis-related cascade(s). SP-STP is classified as a PP2C-type serine/threonine phosphatase based on the conserved signature I–XI motifs (13, 15). The available crystal structures of eukaryotic Ser/Thr phosphatase (15) and that of *Streptococcus agalactiae* (30), and the multiple sequence alignment of PP2C-type serine/threonine phosphatases of major Gram-positive pathogens (supplemental Figs. S3 and S4), have shown that the conserved aspartate residues at positions 18, 36, 192, and 231 (aspartate residues of SP-STP are highlighted in *blue*, Fig. 7*A*) constitute an active catalytic core that can accommodate three $Mn^{2+}$ ions (15, 30). Based on the active site information, we constructed three recombinant SP-STP proteins with single amino acid substitutions, SP-STPD36A, SP-STPD192A, and SP-STPD231A (supplemental Fig. S4, *panels A* and *B*). The catalytic coefficients, $K_m$ and $V_{max}$, revealed that all the mutant STP proteins were catalytically inactive and hence unable to catalyze the *p*-nitrophenyl phosphate dephosphorylation (Fig. 7*B*). Moreover, the SP-STPD192A was incompetent to dephosphorylate Ser/Thr auto-phosphorylated SP-STKK and hence subsequently could not dephosphorylate the Ser/Thr-phosphorylated myelin basic protein (supplemental Fig. S5).

To evaluate the role of phosphatase activity of SP-STP *per se* in mediating its entry into the cytoplasm, pharyngeal cells were treated with the wild-type SP-STP, EF-STP, or the catalytically inactive SP-STPD192A, and their presence within the host cells was detected by Western blot analysis. The results revealed the presence of the anti-SP-STP-reacting 27-kDa protein only in

the whole lysate obtained from the Detroit cells treated with the wild-type SP-STP indicating that neither the enzymatically inactive SP-STPD192A nor EF-STP could enter into the host cell (Fig. 7*C*). Furthermore, these results also indicated that the structure maintained by the catalytic residues is likely essential in mediating the internalization of SP-STP within the pharyngeal cells.

To determine the ability of the internalization-defective mutant protein, SP-STPD192A, along with other catalytic variants, SP-STPD36A and SP-STPD231A, to cause apoptosis of pharyngeal cells, we performed MTT assays on Detroit cells treated with the catalytically inactive mutated proteins. The unaltered proliferation index of Detroit cells treated with the enzymatically inactive proteins (Fig. 7*D*) indicated that the catalytic residues not only impart phosphatase activity to SP-STP but also provide structural framework to the protein facilitating its binding and subsequent internalization in the pharyngeal cells.

### *Structural Framework Maintained by Catalytic Residues of SP-STP Is Essential for Its Entry into Host Cells*

The comparison of the amino acid sequences of EF-STP with that of SP-STP revealed 47% identity and 69% similarity. Furthermore, the enzymatic activity of EF-STP ($K_m$ = 0.125 mM) was also found to be comparable with that of the SP-STP ($K_m$ = 0.35 mM) (13)). Because both catalytically inactive SP-STP and the enzymatically active EF-STP are incompetent to enter into the Detroit cells and hence unable to cause apoptosis (Fig. 7, *B* and *C*), we hypothesized that the specific structure of SP-STP and not the enzymatic activity enables the protein to bind to and enter into the host cells. To explore this, we determined the fractions of secondary structures in both EF-STP and SP-STPD192A proteins using CD spectroscopy. The results highlighted remarkable structural differences in EF-STP (8% $\alpha$-helices and 43% $\beta$-sheets) in comparison with the SP-STP with 37% $\alpha$-helical content and 20% $\beta$-sheets (Fig. 8*A*). Importantly, the catalytically inactive SP-STPD192A showed 13% $\alpha$-helices and 39% $\beta$-sheets, a structure similar to that of EF-STP (Fig. 8, *A* and *B*).

The tertiary structure analysis of the SP-STPD192A mutant protein in comparison with its wild-type SP-STP demonstrated significant conformational rearrangements (transition in the ellipticity from positive to negative) following single amino acid substitution. This suggested that upon alteration of the catalytic Asp-192, the structure of SP-STPD192A protein significantly differs in comparison with its wild-type counterpart and acquires a structural similarity to that of the EF-STP, which was also not able to enter into the cell (Fig. 8*C*).

### *Intracellularly Expressed SP-STP Causes Apoptosis of Pharyngeal Cells*

Because the *stp*-specific transcript was found to be up-regulated in the intracellular GAS population found in Detroit 562 cells (Fig. 1*D*) and PP2C Ser/Thr phosphatase activity in many eukaryotic cells have been shown to play an important role in apoptosis (16, 29), the internalization and subsequent localization of SP-STP in the nucleus (Fig. 6) incited us to hypothesize that the SP-STP causes apoptosis also from within. To validate

(A)

| Proteins | % Secondary Structure | | |
|---|---|---|---|
| | α-helix | β-sheet | Random coil |
| SP-STP | 37 | 20 | 43 |
| SP-STPD192A | 13 | 39 | 48 |
| EF-STP | 08 | 43 | 48 |

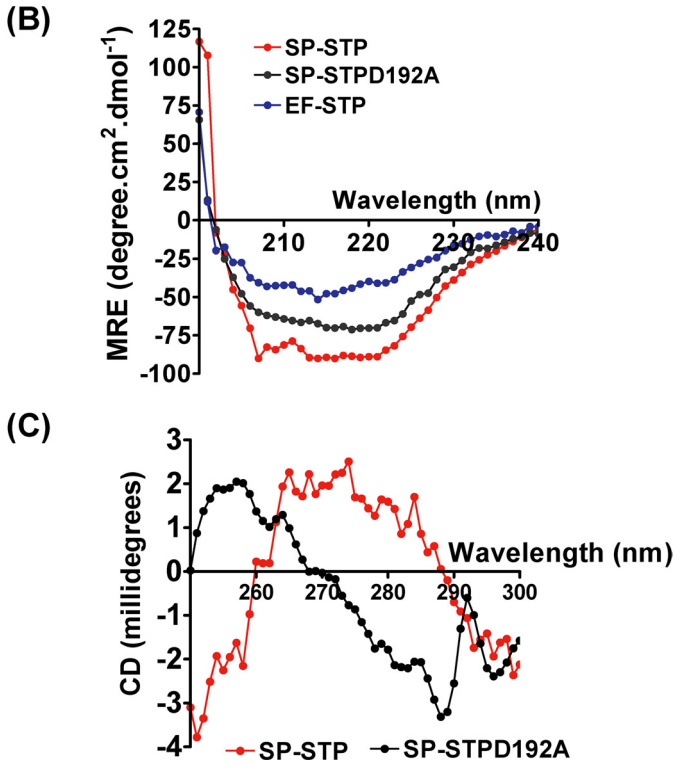


FIGURE 8. *A*, tabulated; *B*, graphical presentation of the results showing the secondary structure determination for wild-type SP-STP, SP-STPD192A, and EF-STP as determined by CD spectroscopy. *MRE*, mean residue ellipticity. *C*, tertiary structural changes in the wild-type and SP-STPD192A as determined using CD spectroscopy.

this, SP-STP was ectopically expressed within Detroit 562 pharyngeal cells, and was confirmed by Western blotting using anti-FLAG and anti-SP-STP antibodies (Fig. 9*A*, *Panel I*). At 72 h post-transfection, the cells expressing STP-FLAG showed prominent signs of apoptosis and started to detach from the surface unlike the cells transfected with the empty pCMV-*FLAG* vector and untreated pharyngeal cells. The MTT assay revealed proliferation inhibition in the cells expressing STP-FLAG in a time-dependent manner (Fig. 9*B*), thereby confirming that the intracellular SP-STP expression also plays a role in causing apoptosis of the pharyngeal cells. In agreement with the inability of the SP-STPD192A mutant to internalize the pharyngeal cells, the ectopic expression of this catalytically inactive variant within the host cells (Fig. 9*A*, *Panel II*) was also not able to significantly affect the proliferation (Fig. 9*B*) of Detroit cells reiterating the key role of the phosphatase activity of SP-STP in causing apoptosis of human pharyngeal cells.

To further validate our observation on the migration of exogenously added SP-STP to the nucleus, we initially attempted to

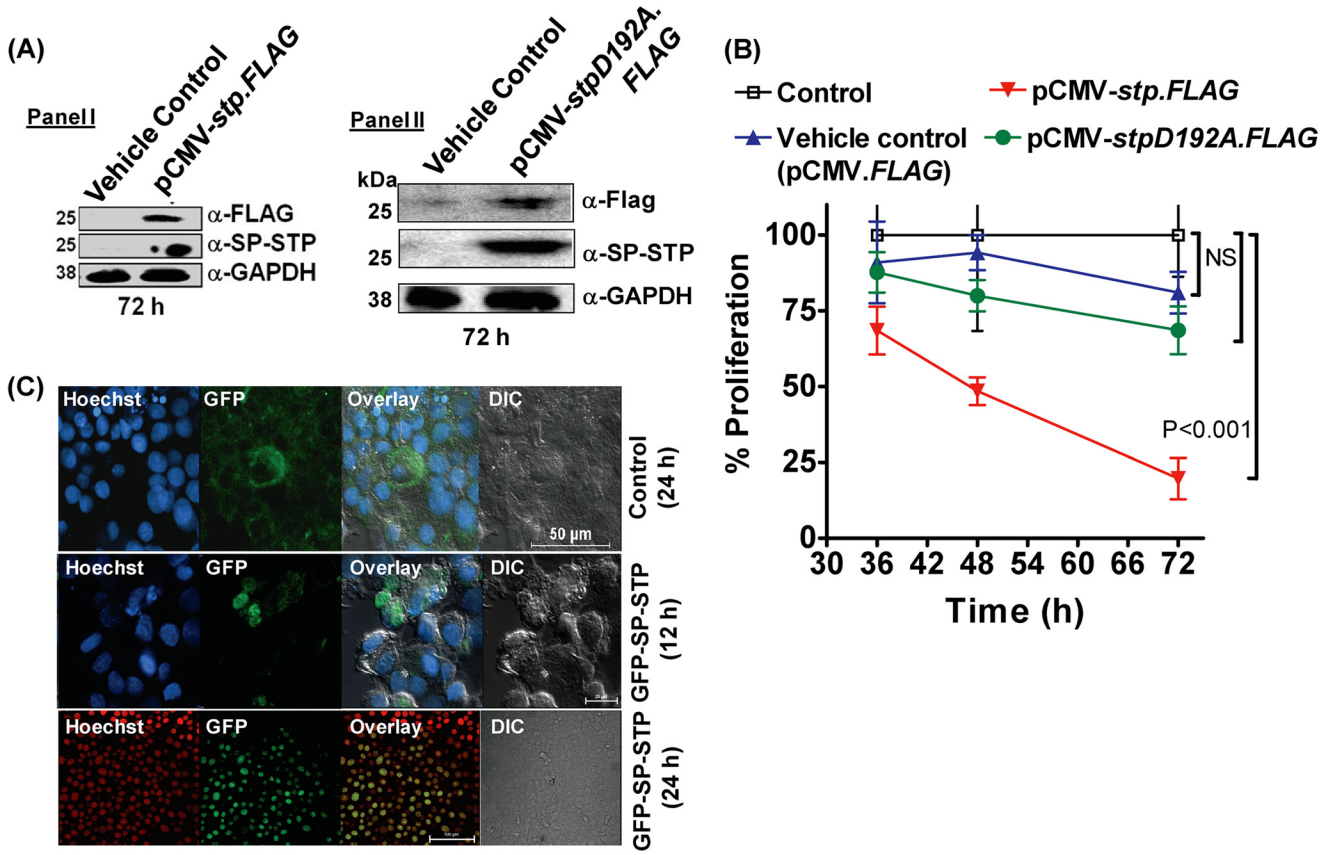


FIGURE 9. *A,* Western blot analysis using anti-FLAG and anti-SP-STP antibodies to depict the expression of STP-FLAG (*Panel I*) and SP-STPD192A (*Panel II*) 72 h post-transfection in Detroit 562 cell lysates. *B,* MTT assay depicting the proliferation index of the Detroit 562 cells transfected with pCMV-*FLAG* (vehicle control), pCMV.*stp-FLAG,* and pCMV-*stpD192A.FLAG* at the indicated time points. *C,* confocal microscopic differential interference contrast (*DIC*) and merged images showing cytoplasmic localization of GFP (24 h) and nuclear localization of SP-STP-GFP (12 and 24 h). Nucleus is stained with Hoechst33342. *Blue DAPI* was changed to the *red channel* for clarity of the superimposed images.

determine the localization of the intracellularly expressed STP-FLAG in the transfected cells using anti-FLAG antibody in an immunofluorescence assay. However, detection of several cross-reactive proteins using anti-FLAG antibody discouraged us from making further attempts in this direction. Hence, we employed an alternative approach by constructing GFP-SP-STP chimera and investigated the fate of the endogenously expressed GFP-linked SP-STP in Detroit 562 pharyngeal cells. As expected, the transfected Detroit 562 cells revealed progressive migration of GFP-SP-STP from the cytoplasm into the nucleus within 24 h (Fig. 9*C*). Concomitant to this event, the transfected cells were found to be rounded with condensed chromatin, indicating that cells had undergone apoptosis. Control cells expressing GFP alone appeared healthy. In these cells, the GFP protein was detected only in the cytoplasm. Taken together, these results thus conclusively proved that SP-STP causes apoptosis of Detroit pharyngeal cells from both without and within. These results further indicated that SP-STP and its catalytic phosphatase activity contributes significantly both extrinsically and intrinsically to the GAS-mediated apoptosis.

### *SP-STP Treatment Affects Transcriptome of Human Pharyngeal Cells*

Because SP-STP progressively migrates from the cytoplasm and enters the host cell nucleus, we envisioned that its presence in both the cellular compartments is likely to trigger a number of intricate cell death-inducing pathways that subsequently culminate into apoptosis. For this, we performed human gene microarray-based differential global gene expression analysis for Detroit pharyngeal cells treated with SP-STP for 6 h. A total of 1,387 were found to be up- or down-regulated by at least 2-fold (188 genes at least 4-fold and 36 genes 8–36-fold). The most notable apoptotic genes (8–36-fold) that were found to be up-regulated were CCL20 and IL-8. Cytochrome P450 and Mir21 were among the most significantly down-regulated genes (Table 1 and supplemental Fig. S6).

To validate these initial findings and to gain an insight into the proteins involved in SP-STP-mediated apoptosis, the qRT-PCR-based gene expression profile for a total of 84 pro- and anti-apoptotic genes was analyzed at three different time intervals (12, 24, and 36 h) representing the early, mid, and late phases of apoptosis post-SP-STP (0.5 $\mu$M) treatment. Fold increase or decrease in the expression levels of several pro- and anti-apoptotic genes, respectively, upon SP-STP treatment is summarized in Table 2.

### *SP-STP-induced Cell Death Involves Activation/Inhibition of Several Pro-/Anti-Apoptotic Factors*

*Role of TNF-α in SP-STP-induced Apoptosis*—The several-fold up-regulation of the TNF-α transcript (Table 2) corroborated with an increase in the TNF-α production after SP-STP

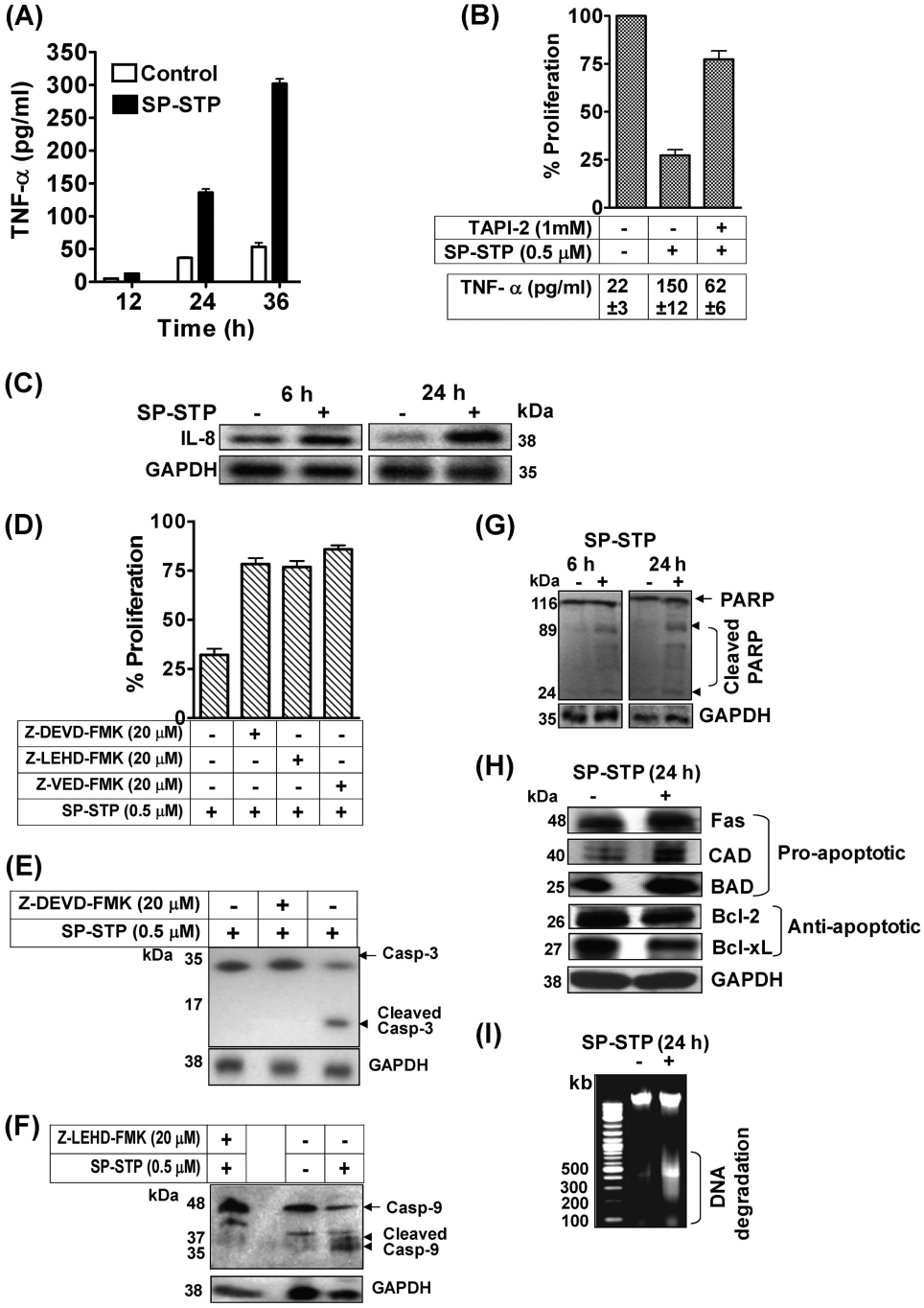


FIGURE 10. *A,* quantitation of TNF-α released upon SP-STP addition by ELISA. *B,* effect of TNF-α inhibitor, TAPI-2, on the SP-STP-induced release of TNF-α from and apoptosis of Detroit 562 cells as revealed by MTT assay. The proliferation of cells treated with the inhibitor alone was taken as control. The *table* below the graph depicts the amount of TNF-α released (in picograms/ml) from the untreated, SP-STP-treated, and TAPI-2-treated Detroit 562 human pharyngeal cells. *C,* Western blot analysis showing changes in the expression of IL-8 after 6 and 24 h of treatment. *D,* effect of caspase inhibitors on the SP-STP-mediated apoptosis of Detroit 562 as determined by MTT assay. *E* and *F,* SP-STP-induced cell death is caspase-dependent. Western blots depicting the SP-STP induced cleavage of caspase-3 (*E*) and caspase-9 (*F*) in the presence and absence of specific inhibitors. The proliferation of cells treated with the inhibitors alone in each case was taken as control. *G,* Western blot depicting the cleavage of PARP after 6 and 24 h post-SP-STP addition. *H,* Western blot analysis showing the changes in the expression of indicated pro- and anti-apoptotic proteins using specific antibodies as described. The GAPDH was used as loading control. *I,* ethidium bromide-stained 0.8% agarose gel showing DNA fragmentation patterns in SP-STP-treated (+) and untreated (−) pharyngeal cells. The *first lane* depicts the migration pattern of the DNA molecular weight ladder.

addition in a time-dependent fashion (Fig. 10*A*). To assess the role of TNF-α in SP-STP-induced apoptosis, the cells were incubated with TNF-α inhibitor, TAPI-2, prior to SP-STP addition. The MTT assay revealed that the cells that were incompetent to produce TNF-α failed to display apoptosis (Fig. 10*B*). The amount of TNF-α (in picograms/ml) was also estimated to ensure that this reduction in proliferation inhibition is indeed due to the inability of cells to produce TNF-α. The amount of TNF-α produced upon 24 h of SP-STP addition was found to be only 62 ± 6 pg/ml in TAPI-2-treated cells as opposed to 150 ± 12 pg/ml in the absence of inhibitor (without TAPI-2). This clearly indicates that TNF-α induction upon SP-STP exposure

**TABLE 1**

**Microarray analysis showing highly differentiated human gene expression in Detroit 562 cells treated with SP-STP**

Results are obtained with two independent experiments each for Detroit 562 cells untreated and SP-STP-treated cells (0.5 $\mu$M) for 6 h. Data were analyzed using ArrayStar4 microarray analysis software.

| Affymetrix Probe Set ID | gene name | Gene function | Fold-change |
|---|---|---|---|
| 205476_at | CCL20 | chemokine (C-C motif) ligand 20 | 35.56 |
| 207850_at | CXCL3 | chemokine (C-X-C motif) ligand 3 | 14.21 |
| 216598_s_at | CCL2 | chemokine (C-C motif) ligand 2 | 3.17 |
| 217028_at | CXCR4 | chemokine (C-X-C motif) receptor 4 | 3.60 |
| 206336_at | CXCL6 | chemokine (C-X-C motif) ligand 6 (granulocyte chemotactic protein 2) | 4.62 |
| 204470_at | CXCL1 | chemokine (C-X-C motif) ligand 1 (melanoma growth-stimulating activity, alpha) | 5.86 |
| 209774_x_at | CXCL2 | chemokine (C-X-C motif) ligand 2 | 6.41 |
| 214683_s_at | CLK1 | CDC-like kinase 1 | 5.34 |
| 211506_s_at | IL8* | interleukin 8 | 15.63 |
| 205207_at | IL6 | interleukin 6 | 4.23 |
| 202644_s_at | TNFAIP3 | tumor necrosis factor, alpha-induced protein 3 | 4.830 |
| 221085_at | TNFSF15 | tumor necrosis factor (ligand) superfamily, member 15 | 2.22 |
| 202644_s_at | TNFAIP3 | tumor necrosis factor, alpha-induced protein 3 | 4.83 |
| 212665_at | TIPARP | TCDD-inducible poly(ADP-ribose) polymerase | 7.66 |
| 205027_s_at | MAP3K8 | mitogen-activated protein kinase kinase kinase 8 | 4.99 |
| 235086_at | THBS1 | Thrombospondin 1 | 6.80 |
| 214451_at | TFAP2B | transcription factor AP-2 beta (activating enhancer binding protein 2 beta) | 3.49 |
| 1559975_at | BTG1 | B-cell translocation gene 1, anti-proliferative | 15.18 |
| 222162_s_at | ADAMTS1 | ADAM metallopeptidase with thrombospondin type 1 motif, 1 | 14.36 |
| 241716_at | HSPD1 | heat shock 60kDa protein 1 (chaperonin) | 13.82 |
| 208892_s_at | DUSP6 | dual specificity phosphatase 6 | 11.68 |
| 222486_s_at | ADAMTS1 | ADAM metallopeptidase with thrombospondin type 1 motif, 1 | 11.17 |
| 210335_at | RASSF9 | Ras association (RalGDS/AF-6) domain family (N-terminal) member 9 | 10.21 |
| 202207_at | ARL4C | ADP-ribosylation factor-like 4C | 9.83 |
| 207345_at | FST | follistatin | 9.02 |
| 203821_at | HBEGF | heparin-binding EGF-like growth factor | 8.90 |
| 204995_at | CDK5R1 | cyclin-dependent kinase 5, regulatory subunit 1 (p35) | 2.56 |
| 210189_at | HSPA1L | heat shock 70kDa protein 1-like | 8.13 |
| 207530_s_at | CDKN2B¶ | cyclin-dependent kinase inhibitor 2B (p15, inhibits CDK4) | -2.941 |
| 218929_at | CDKN2A | CDKN2A interacting protein | -4.209 |
| 236313_at | CDKI2B | cyclin-dependent kinase inhibitor 2B (p15, inhibits CDK4) | -2.026 |
| 226530_at | BMF | Bcl2 modifying factor | -3.014 |
| 232746_at | CXCR7 | Chemokine (C-X-C motif) receptor 7 | -3.796 |
| 204475_at | MMP1 | matrix metallopeptidase 1 (interstitial collagenase) | -2.456 |
| 204933_s_at | TNFRSF11B | tumor necrosis factor receptor superfamily, member 11b (osteoprotegerin) | -8.7 |
| 1569003_at | TMEM49 | transmembrane protein 49 | -10.62 |
| 205749_at | CYP1A1 | cytochrome P450, family 1, subfamily A, polypeptide 1 | -5.79 |
| 1568868_at | CYP27C1 | cytochrome P450, family 27, subfamily C, polypeptide 1 | -3.88 |
| 202434_s_at | CYP1B1 | cytochrome P450, family 1, subfamily B, polypeptide 1 | -2.26 |
| 238909_at | S100A10 | S100 calcium binding protein A10 | -15.73 |
| 224917_at | MIRN21 | microRNA 21 | -22.27 |

¶ Shaded rows indicate down-regulated genes.

is a key event that facilitates subsequent induction of the apoptotic cascade.

In addition to TNF-$\alpha$, IL-8, a pro-inflammatory cytokine, has been shown to be induced in response to TNF-$\alpha$ production and FAS ligation to augment apoptosis (31). The substantial induction of mRNA corresponding to IL-8 (15.6-fold) in pharyngeal cells treated with SP-STP within 6 h as assessed by microarray analysis (Table 1) corroborated with the observed up-regulation of IL-8 protein in cells treated with SP-STP as early as 6 h and also at later (24 h) time point (Fig. 10*C*).

*SP-STP-mediated Apoptosis Is Caspase-dependent*—The activation of initiator caspase (caspase-10, 2-fold, Table 2),

**TABLE 2**

**Real time PCR analysis showing highly differentiated apoptosis-related genes in Detroit 562 human pharyngeal cells treated with SP-STP for indicated time intervals**

The columns showing a dash indicate the absence of the detectable transcript in that time period. Shaded regions depict the fold down-regulation of anti-apoptotic genes. The gene functions are mentioned as reported in the SABiosciences (PAHS-012A) custom-made apoptotic PCR array.

| Gene name | Gene function | Linear Fold Change ± S.D | | |
|---|---|---|---|---|
| | | 12 h | 24 h | 36 h |
| BNIP 1 | BCL2/adenovirus E1B 19kDa interacting protein 1 | - | - | 2.2 ± 0.30 |
| BNIP 2 | BCL2/adenovirus E1B 19kDa interacting protein 2 | - | - | 2.3 ± 0.25 |
| BNIP 3 | BCL2/adenovirus E1B 19kDa interacting protein 3 | 2.50 ± 0.20 | 4.20 ± 1.00 | - |
| CASP1 | Caspase 1, apoptosis-related cysteine peptidase (interleukin 1, beta, convertase) | - | 2.20 ± 0.40 | - |
| CASP3 | Caspase 3, apoptosis-related cysteine peptidase | - | - | 2.0 ± 0.27 |
| CASP4 | Caspase 4, apoptosis-related cysteine peptidase | | 2.10 ± 0.25 | - |
| CASP5 | Caspase 5, apoptosis-related cysteine peptidase | 2.30 ± 0.60 | 4.00 ± 0.90 | 2.1 ± 0.20 |
| CASP9 | Caspase 9, apoptosis-related cysteine peptidase | - | - | 2.3 ± 0.30 |
| CASP10 | Caspase 10, apoptosis-related cysteine peptidase | 2.10 ± 0.50 | - | - |
| CASP14 | Caspase 1, apoptosis-related cysteine peptidase | - | 3.00 ± 0.30 | - |
| TNF | Tumor necrosis factor | 9.50 ± 1.20 | 31.00 ± 3.50 | 78.0 ± 5.60 |
| TNFRSF10A | Tumor necrosis factor receptor superfamily, member 10a | 2.30 ± 0.30 | - | 2.3 ± 0.45 |
| TNFRSF9 | Tumor necrosis factor receptor superfamily, member 9 | 10.00 ± 1.80 | 6.00 ± 1.80 | 16.0 ± 2.10 |
| TNFRSF10 | Tumor necrosis factor receptor superfamily, member 10a | 2.10 ± 0.25 | 2.40 ± 0.40 | - |
| TNFRSF10B | Tumor necrosis factor receptor superfamily, member 10b | - | - | 4.3 ± 1.50 |
| TNFRSF11B | Tumor necrosis factor receptor superfamily, member 11b | - | - | 3.0 ± 1.40 |
| TNFSF8 | Tumor necrosis factor (ligand) superfamily, member 8 | - | 5.50 ± 1.60 | - |
| CD40LG | CD40 ligand | - | 10.00 ± 2.10 | - |
| CD40 | CD40 molecule, TNF receptor superfamily member 5 | 2.80 ± 0.12 | 3.30 ± 0.60 | 3.2 ± 1.00 |
| CD27 | CD27 molecule | - | 4.30 ± 1.50 | - |
| CD70 | CD70 molecule | 3.20 ± 0.30 | 3.50 ± 0.80 | 4.1 ± 1.60 |
| FAS | Fas (TNF receptor superfamily, member 6) | 2.40 ± 0.20 | - | - |
| FASLG | Fas ligand (TNF superfamily, member 6) | - | 10.00 ± 2.00 | - |
| LTA | Lymphotoxin alpha (TNF superfamily, member 1) | 3.50 ± 0.30 | 16.00 ± 2.00 | 6.1 ± 1.30 |
| RIPK2 | Receptor-interacting serine-threonine kinase 2 | 2.60 ± 0.15 | - | - |
| TP53BP2 | Tumor protein p53 binding protein, 2 | - | - | 5.2 ± 1.80 |
| TRAF4 | TNF receptor-associated factor 4 | - | - | 2.1 ± 0.22 |
| GADD45A | Growth arrest and DNA-damage-inducible, alpha | - | - | 10.0 ± 2.60 |
| CFLAR | CASP8 and FADD-like apoptosis regulator | 2.20 ± 0.50 | 3.50 ± 0.50 | 3.4 ± 0.50 |
| BCL2L10 | BCL2-like 10 (apoptosis facilitator) | - | 6.50 ± 1.50 | 4.8 ± 1.50 |
| BIK | BCL2-interacting killer-apoptosis inducing | - | 5.00 ± 1.30 | - |
| BAG4 | BCL2-associated athanogene 4 | - | 2.6 ± 0.3 | - |
| BCL2L2 | BCL2-like 2 | - | 2.0 ± 0.5 | - |
| NAIP | NLR family, apoptosis inhibitory protein | - | - | 4.0 ± 0.75 |
| ABL-1 | C-abl oncogene 1, non-receptor tyrosine kinase | - | - | 2.5 ± 0.6 |
| IGF1R | Insulin-like growth factor 1 receptor | - | - | 4.2 ± 0.45 |
| MCL-1 | Myeloid cell leukemia sequence 1 (BCL2-related) | - | - | 2.0 ± 0.05 |
| CASP2 | Caspase 2, apoptosis-related cysteine peptidase | - | 3.5 ± 0.4 | 4.5 ± 0.23 |
| AKT-1 | V-akt murine thymoma viral oncogene homolog 1 | - | 2.3 ± 0.2 | 3.4 ± 0.2 |

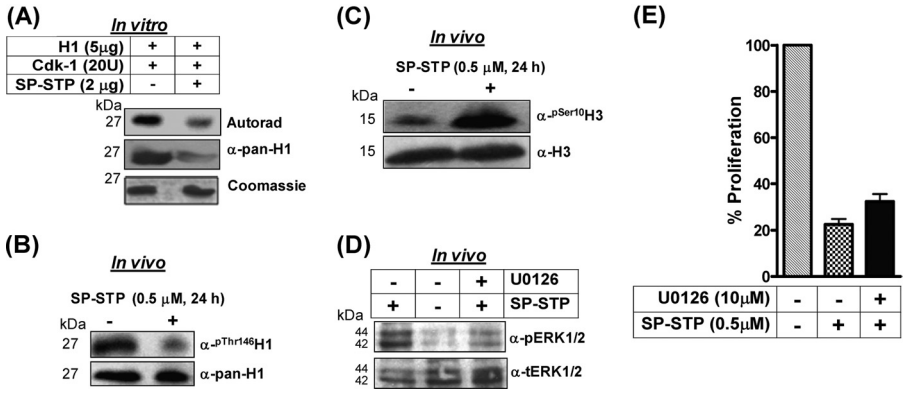


FIGURE 11. *A,* autoradiogram and Coomassie staining showing the ability of SP-STP to dephosphorylate the CDK-1-phosphorylated histone H1 *in vitro*. The identity of the samples was ascertained by immunoblotting using anti-pan-H1 antibody. *B, in vivo* analysis of H1 phosphorylation in the nuclear extracts isolated from the control and SP-STP-treated pharyngeal cells using anti-phospho-Thr$^{146}$-H1 ($\alpha$-$^{Thr(P)-146}$H1) antibody. Anti-H1 antibody-reactivity ($\alpha$-pan-H1) was used as the loading control. *C,* anti-H3-Ser(P)$^{10}$ antibody ($\alpha$-$^{Ser(P)-10}$-H3) reactivity showing histone H3 phosphorylation in the nuclear extracts of the SP-STP-treated and -untreated (control) pharyngeal cells. Anti-H3 antibody reactivity (Nu-H3) was used as the loading control. *D,* Western blot analysis depicting the change in the phospho-ERK1/2 (pERK1/2) profile in the untreated and SP-STP-treated pharyngeal cells alone or in the presence of the ERK1/2 inhibitor, U0126. The level of total ERK1/2 (tERK1/2) was taken as the loading control. *E,* MTT assay showing the SP-STP induced-proliferation inhibition of Detroit 562 cells in the presence and absence of ERK1/2 inhibitor U0126. The proliferation of cells treated with the inhibitor alone was taken as control.

which belongs to the extrinsic apoptotic pathway as early as 12 h of SP-STP treatment, indicated the initiation of early apoptotic events upon SP-STP treatment. However, the increased expression of executioner caspases, caspase-3 (2-fold, Table 2) and caspase-9 (2.3-fold, Table 2), upon SP-STP treatment was observed only at the later time point (36 h, Table 2). Western blot analysis showing increased amounts of the cleaved products of these executioner caspases confirmed their activation upon SP-STP treatment of Detroit 562 cells (Fig. 10, *E* and *F*). To further validate the role of caspases in STP-induced cell death, the pharyngeal cells were preincubated with caspase-3, caspase-9, and general caspase inhibitors. The cell death in each case was monitored by MTT assays. The data revealed that the addition of all the caspase inhibitors markedly abrogated the SP-STP-induced cell death (Fig. 10*D*). The inability of the caspase-3 and caspase-9 to cleave to their active forms in the presence of the specific inhibitors as assessed by Western blotting (Fig. 10, *E* and *F*) also substantiated the involvement and activation of caspases as a prerequisite in SP-STP-mediated apoptosis of human pharyngeal cells.

Furthermore, the cleavage of poly-ADP-ribose polymerase (PARP), as early as 6 h and at 24 h in SP-STP-treated pharyngeal cells as assessed by Western blot analysis (Fig. 10*G*), also correlated well with transcription profiling of the *parp* gene in SP-STP-treated pharyngeal cells (8-fold, microarray analysis, Table 1). Caspase-3 activation and PARP cleavage have been shown to prevent DNA repair and promote internucleosomal DNA cleavage/condensation (32). Our observation showing increased expression of 40-kDa CAD, which is a caspase-3-activated DNase (Fig. 10*H*, *2nd row*), and DNA fragmentation ranging from 250 to 500 bp (Fig. 10*I*) suggested that upon SP-STP treatment caspase-3 and PARP activation leading to the increased CAD expression might result in the observed DNA nuclear fragmentation and condensation.

Furthermore, for several relevant pro-apoptotic (FAS, CAD, and BAD)- and anti-apoptotic (Bcl-2 and Bcl-xL)-related genes, we did not observe a detectable signal in the qRT assays. However, the increased and decreased protein expression levels of these pro-apoptotic and anti-apoptotic proteins, respectively, in the SP-STP-treated pharyngeal cells (24 h) indicated the additive effects in conferring apoptosis (Fig. 10*H*). Additionally, the altered expression of several mitochondrial associated proteins, Bcl-2, Bcl-xL Bik, and Mcl-1 at the mRNA and/or protein levels (Fig. 10*H* and Table 1), corroborated with the observed phenotypical and biochemical changes (Figs. 2 and 4) in the mitochondria of SP-STP-treated Detroit 562 pharyngeal cells. Together, these results indicated that SP-STP-mediated apoptosis of pharyngeal cells is an outcome of several up-regulated pro-apoptotic and down-regulated anti-apoptotic factors.

### *Histones, Possible Downstream Targets of SP-STP-mediated Apoptotic Signaling*

Phosphorylation and dephosphorylation of histones are essential events regulating cell cycle progression and associated structural changes in the chromatin (33, 34). In light of the above results, especially the observed chromatin condensation of SP-STP-treated Detroit pharyngeal cells (Fig. 1) and internalization of SP-STP into the nucleus (Figs. 6 and 9), we speculated that the SP-STP-mediated dephosphorylation might result in chromatin condensation. To validate this hypothesis, we evaluated the potential of SP-STP to dephosphorylate the CDK-1-phosphorylated histone H1 in an *in vitro* kinase assay. Interestingly, we found that the purified SP-STP was able to dephosphorylate the H1~P histone (Fig. 11*A*). This was substantiated by assessing the *in vivo* H1 phosphorylation status in the nuclear extract of SP-STP-treated pharyngeal cells using anti-$^{Thr(P)-146}$H1 antibody. A significant reduction in the reactivity of anti-Pan H1-reacting 27-kDa protein in the nuclear extract obtained from the SP-STP-treated Detroit cells with anti-$^{Thr(P)-146}$H1 antibody (Fig. 11*B*) correlated well with the discernible dephosphorylation of purified H1~P histone by CDK-1 (Fig. 11, *A* and *B*).

Additionally, histone H3 hyperphosphorylation has been considered as the hallmark of apoptosis because it facilitates chromatin condensation (35). The status of H3 phosphorylation in the cells undergoing apoptosis was determined in the

nuclear extracts obtained from the SP-STP-treated pharyngeal cells using anti-$^{Ser(P)-10}$-H3 antibody. An intense immunoreactive band in the SP-STP-treated cells in comparison with the untreated cells (Fig. 11*C*) concurred with the established direct relationship between the hyperphosphorylated H3 and apoptosis. Because MAPK mediates H3 phosphorylation and apoptosis (36), we predicted the activation of ERK1/2 is likely linked to the observed H3 phosphorylation. Consistent with this notion, our results revealed a significant activation of ERK1/2 upon 24 h of SP-STP treatment (Fig. 11*D*). To ascertain the importance of ERK activation in SP-STP-induced cell death, the specific ERK1/2 inhibitor U0126 was added prior to SP-STP addition. The cells were assessed for the level of phosphorylated ERK1/2 as an effect of U0126 addition using Western blotting followed by MTT assay to determine cell death. Although the level of activated ERK (phosphorylated state) was reduced upon U0126 addition (Fig. 11*D*), SP-STP was able to confer apoptosis even in the presence of inhibitor (Fig. 11*E*). Together, these results suggest that ERK activation and subsequent histone H3 phosphorylation are some of the effects of SP-STP-induced apoptosis but not the primary cause of SP-STP-mediated apoptosis.

Collectively, the results obtained in this study unequivocally establish the potential role of SP-STP in interfering with the host cell signaling events by activating both the extrinsic (death receptors on the cell surface) apoptotic pathways subsequent to its binding to the pharyngeal cells and intrinsic (caspase activation and mitochondrial impairment) pathways upon its internalization and transmigration into the nucleus.

## DISCUSSION

Although the function of eukaryote-like serine/threonine kinases in bacterial virulence has been established, the precise biological functions of its co-transcribing phosphatase, SP-STP in GAS, and the structural homologs found in other pathogens are not known (26). The ubiquitous existence of these modules in a variety of prokaryotes, including pathogens, indicates that the pathogens might use these proteins to exploit the host signaling system for their own advantage. Eukaryote-type STK, being a transmembrane protein with its kinase domain restricted within the cytoplasm (13), is unlikely to interfere with the host cell signaling. However, SP-STP, secreted from GAS (13), potentially has a significant role in interfering and even disrupting the host cell signaling events during active GAS infection. Our recent finding demonstrating SP-STP as an essential protein required for the maintenance and regulation of GAS virulence (14) provided a requisite impetus to investigate the direct biological function of SP-STP affecting the host cells. In this study, we systematically delineated the precise role of SP-STP in GAS pathogenesis.

The preliminary clue that initiated this investigation stems from the observed up-regulation of the mRNA expression of SP-STP encoding gene (*SPy1626*) as assessed by the global gene expression analysis of the GAS population exclusively isolated from the pharyngeal cells. This prompted us to determine the direct consequence of SP-STP addition on human pharyngeal cells. Although the direct binding of SP-STP to Detroit 562 cells indicated that the purified SP-STP is capable of causing apoptosis of the host cells, its role as a sole contributor in GAS-mediated apoptosis remains debatable because at least two other well established toxins, Nga/Spn and SpeB, have also been shown to possess similar implications in OKP7 keratinocytes/J774 macrophage cells and A594 epithelial/U937 monocytic cells, respectively (11, 12, 37, 38). However, it has also been reported that 20 $\mu$g of exogenously added SpeB could bring about only 12 and 17% inhibition of cell proliferation after 24 h and 48 h of treatment, respectively, in U937 human monocytic cells (12). In A594 epithelial cells, it has been shown that SpeB was not required for induction of apoptosis by GAS-infected epithelial cells (39). Our data showing the ability of SP-STP to inhibit 75% of cell proliferation in A594 cells at 0.5 $\mu$M within 24 h reflect the potency of SP-STP to induce apoptosis. Additionally, our recent findings using SP-STP knock-out mutants derived from M1SF370 and M1T15448 GAS strains indicated differential *speB* and *nga* expression and related invasive properties in an *in vitro* invasion assay (14). Despite the fact that *speB* was highly up-regulated (16-fold) in the M1ΔSTP mutant and down-regulated (13-fold) in M1T1ΔSTP mutant, and *nga* was unaltered in M1ΔSTP and highly up-regulated (>50-fold) in M1T1ΔSTP (14), these mutants were incompetent to cause apoptosis (no inhibition in proliferation) (Fig. 3*B*) indicating that neither SpeB nor Nga plays a significant role in causing apoptosis of human pharyngeal cells. Also, it is important to note that the Nga/Spn and Slo has been shown to exert cytotoxic effects on the keratinocytes during GAS infection, but its expression cannot be generally/usually correlated directly with the pathogenicity because many pathogenic strains, including M1SF370, express enzymatically inactive Spn (40). In this regard, as reported recently, Slo is able to cause apoptosis of human macrophages and abrogating innate immune responses (11). It is however not known whether Slo confers apoptosis as an outcome of its ability to form pores in the host cell membrane and cytotoxic activity (37, 41).

The secretion of SP-STP and up-regulation of *stp*-specific transcript upon GAS invasion has been envisioned to provide bimodal contribution to GAS-mediated apoptosis. During adherence, the secreted SP-STP from adherent GAS can cause apoptosis from without possibly through receptor-mediated internalization. However, the significant up-regulation of SP-STP in the intracellular GAS population endorses the likelihood of GAS-mediated apoptosis from within. Although we showed the progressive migration of SP-STP from the cell surface to the cytoplasm, the inability of enzymatically active EF-STP to internalize and cause apoptosis, despite the fact that the PP2C family members of Gram-positive pathogens share high sequence similarity, was quite intriguing. Interestingly, we observed that a single amino acid substitution in the active site pocket of SP-STP resulted in substantial alteration in the folding of the mutant protein (SP-STPD192A). A 2-fold increase in the $\beta$-sheets and 3-fold decrease in the $\alpha$-helical contents with a small gain in the random coils (reflecting disorder) in the SP-STPD192A was quite similar to the structure of EF-STP, which was also not able to internalize and cause apoptosis of pharyngeal cells. Thus, this observed close similarity in the structures of SP-STPD192A and EF-STP is suggestive of the loss or absence of required structure involved in receptor bind-

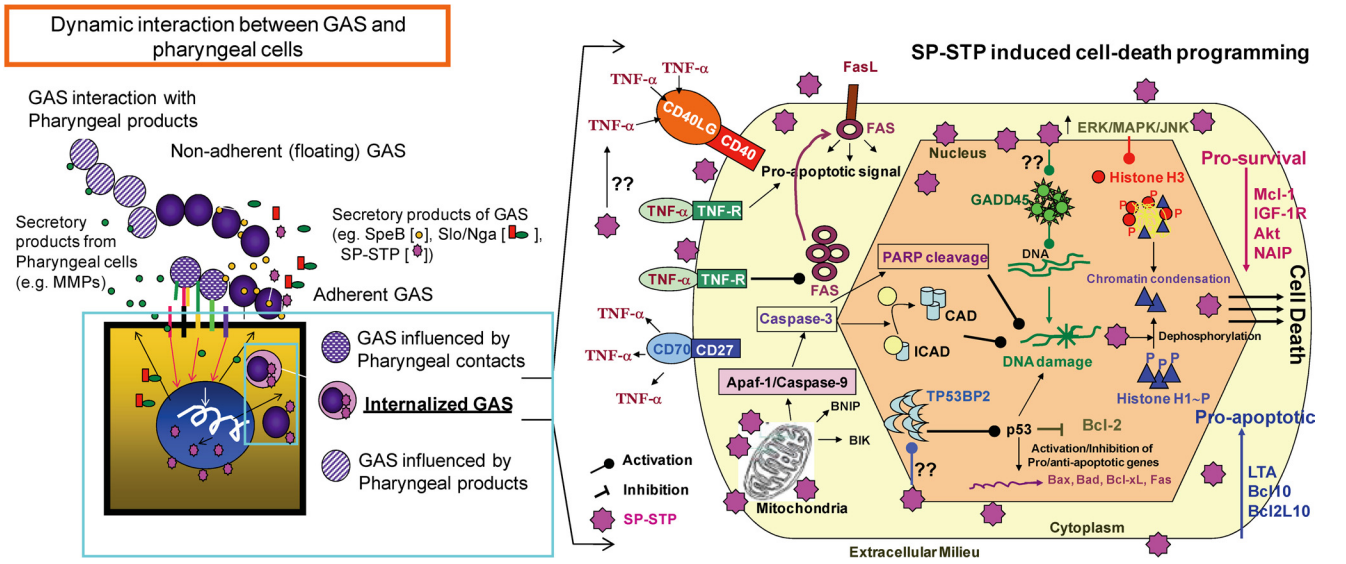


FIGURE 12. **Model depicting the up-/down-regulation of pro-/anti-apoptotic cascades in both the cytoplasmic and nuclear compartments of the Detroit 562 human pharyngeal cells upon SP-STP treatment.** GAS responds to the external environment. Hence the genes expression repertoire in GAS varies according to the constantly changing environments within the host. As a result, the gene expression profiles of the GAS population not in contact with the host cells (floating/non adherent GAS) *versus* the GAS population in contact with the host cells (adherent GAS) *versus* those that are found within the host cells (invaded GAS) are quite different. We found that the GAS found exclusively within the host cells is highly virulent as many virulence and virulence-regulating genes are up-regulated. Among them, eukaryote-like Ser/Thr phosphatase (SP-STP) is the focus of this study, which has been reported previously as a secretory protein. SP-STP, by virtue of its eukaryote-type nature and its overexpression within the cytoplasm of pharyngeal cells upon GAS invasion, becomes a promiscuous protein exploited by GAS to hijack host signal transduction cascades both extrinsically, *i.e.* when it is secreted from the adherent GAS, and intrinsically, when it is secreted in large amounts by the intracellular invaded GAS. We demonstrate that the final destination of SP-STP whether from outside or inside is the host cell nucleus. The Ser/thr phosphatase activity of SP-STP directly or indirectly activates expression of several pro-apoptotic genes and suppresses anti-apoptotic genes. The cumulative effects of these processes culminate in mitochondrial malfunctioning, changes in histone phosphorylation status, chromatin fragmentation, and condensation. Ultimately these changes result in apoptosis and proliferation inhibition of pharyngeal cells. SP-STP thus significantly contributes to the GAS-mediated apoptosis.

ing and is also to gain an entry into the pharyngeal cells and cause apoptosis.

This study also elucidates the SP-STP-induced signaling cascade within the pharyngeal cells that culminates in programmed cell death (Fig. 12). Our findings revealed a substantial up-regulation of tumor necrosis factor-α (TNF-α), a pleiotropic cytokine (43), in pharyngeal cells both at mRNA and protein levels (Fig. 10*A* and Table 2). The concomitant overexpression of TNF-α receptor (TNFRFSF9) and the activation of initiator caspase-10 as early as 12 h of SP-STP treatment (Table 2) provide a clear indication of initiation of an early apoptotic cell death pathway (44). Because CD40-CD40L engagement is implicated in inducing expression of FAS/FAS-L on the cell surface thereby mediating apoptosis in hepatocytes (45), the observed up-regulation of both the members of TNF receptor superfamily (CD40 and FAS, 3-fold; CD40L and FAS-L, 10-fold) also signifies an important role of SP-STP in inducing extrinsic apoptotic cascade in the human pharyngeal cells from without.

Mitochondrial intactness both at the structural and functional levels is a prerequisite for cell survival. Mitochondrial membrane depolarization has been demonstrated to occur via the induction of TNF-α followed by BNIP3 induction (43) or by BIK induction that disrupts calcium homeostasis in endoplasmic reticulum perturbation of mitochondrial membrane permeability (46). Our results showing up-regulation of certain key pro-apoptotic factors belonging to the BCL2 family (2.5–4-fold BNIP3 and 5-fold BIK), along with TNF-α induction concomitant with significant loss of mitochondrial membrane polarization upon SP-STP treatment, support this established mechanism of mitochondrial dysfunctioning as one of the important signaling events leading to the apoptosis of pharyngeal cells.

Besides perturbation in the mitochondrial membrane permeability, Akt1 and caspase-9 play a central role in DNA damage that ultimately leads to chromatin condensation and apoptosis (47). Activation of ERK1/2 and down-regulation of Mcl-1 are directly associated with down-regulation of Akt1 (48). The latter has been shown to mediate phosphorylation of caspase-9 and suppress apoptosis in human cell lines (47). In addition to caspase-9, caspase-9 activator Apaf1, and caspase-9 suppressors XIAP and BAD are the well established targets of Akt1-mediated phosphorylation that exert anti-apoptotic effects. Thus, the down-regulation of Akt1 or its dephosphorylation, such as by PTEN, allows Apaf1 to remain phosphorylated, which in turn activates caspase-9. The latter subsequently activates procaspase-3 and procaspase-7, which cleave several cellular targets, including PARP, and thus promotes DNA damage ultimately leading to enhanced apoptosis (47). Our observation at the mRNA and/or protein levels revealing significant up-regulation of ERK1 and concomitant down-regulation of Akt1, Mcl-1 (anti-apoptotic proteins), and up-regulation of BAD and caspase-9 upon SP-STP treatment of human Detroit 562 pharyngeal cells correlates well with the regulation of above-mentioned classical apoptotic pathway. Our observation revealing up-regulation of 53BP2 (tumor suppressor p53-binding protein 2, 5-fold), GADD45A (Growth Arrest and DNA Damage-inducible protein, 10-fold), down-regulation of NAIP (Neural Apoptosis Inhibitory Protein, a known inhibitor of caspase-3

and-7), along with caspase-9 and PARP activation, in SP-STP-treated pharyngeal cells provides evidence for another possible mechanism of membrane depolarization. This is true as 53BP2 has been shown to complex with BCL2 and induces apoptosis by de-repression of the mitochondrial membrane potential ($\Psi_m$) and caspase-9 activation (49), which in turn promotes DNA damage following PARP cleavage.

The most remarkable highlight of this investigation is the ability of SP-STP to traverse specifically through two membrane barriers and enter into the nucleus of the pharyngeal cell to mediate apoptosis. The presence of SP-STP within the nucleus of pharyngeal cells prompted us to postulate that SP-STP by virtue of its Ser/Thr phosphatase (dephosphorylation) activity may interface and hijack several host signaling pathways and program them for apoptosis. Thus, SP-STP may dephosphorylate critical host nuclear proteins. Because histones and their post-translationally modified forms play a fundamental role in maintaining the integrity of chromatin structure (50), we envisaged that the SP-STP-mediated histone modification events are likely related to the observed morphological nuclear changes (chromatin condensation and DNA fragmentation) occurring in pharyngeal cells undergoing apoptosis. Congruent with the histone-H1 dephosphorylation in either TNF-$\alpha$ or stress-induced apoptosis and the role of PP1-type phosphatase to dephosphorylate H1 (33–36), our findings showing the ability of SP-STP to dephosphorylate CDK-1 *in vitro*, a nuclear kinase responsible for histone phosphorylation, prompted us to investigate the effect of SP-STP on histone dephosphorylation. The H1 dephosphorylation leading to aberrant chromatin condensation and the hyperphosphorylation of H1 (by cdc2 kinase) in actively dividing cells (33–36) suggest the existence of an intricate balance and fine-tuning between cell division and growth arrest. The dephosphorylated state of H1 linker histone in SP-STP-treated cells is therefore likely to modulate the transcriptome in a way that promotes cell death.

Contrary to H1 dephosphorylation, histone H3 phosphorylation at serine and threonine residues, mediated via ERK1/2 pathway, has been implicated in apoptosis by destabilizing the chromatin leading to its decreased DNA binding affinity (35, 36, 51). Thus, the prominent hyperphosphorylation of histone H3 in Detroit 562 pharyngeal cells treated with SP-STP may result in acquisition of substantial negative charge by histone H3. The latter might be sufficient enough to disrupt its electrostatic interactions with the DNA backbone, resulting in distortion of the chromatin assembly, deleterious effects on the transcription, and ultimately apoptosis. However, no inhibition in apoptosis upon blocking this particular pathway (ERK activation) suggests that the induction of ERK phosphorylation and subsequent H3 phosphorylation are downstream events of this apoptotic cascade. The induction of apoptosis and expression of apoptosis-related proteins occur as early as 6 h of SP-STP treatment (Table 1), which precedes its nuclear translocation that occurs at 12–24 h. This observation in conjunction with reports demonstrating the influence of duration, extent, and strength of ERK activation in governing the delicate balance between differentiation and apoptosis (52) suggest that the ERK activation and H3 phosphorylation post-SP-STP treatment are outcomes of the SP-STP addition but possibly not the cause of SP-STP-induced apoptosis.

In conclusion, the up- and down-regulation of several key pro-apoptotic factors and anti-apoptotic factors, respectively, clearly demonstrate that SP-STP, via its dephosphorylation activity and possibly via binding to its putative receptor, interfaces with and modulates several signaling pathways. This, in turn, targets a variety of crucial cellular organelles, causing multifarious deleterious effects and ultimately apoptosis of the host cell. Although invasion of GAS and its persistence within pharyngeal cells have been associated with penicillin treatment failure and recurrent tonsillitis (42), it is not known by what mechanism intracellular GAS are externalized and cause recurrent infection. This study demonstrating the high expression of SP-STP in intracellular GAS and significant contribution of SP-STP to GAS-mediated apoptosis from within highlights the ability of GAS to exploit host machinery for its own advantage to persist and proliferate within host tissue. We believe that our ongoing investigation on the identification of SP-STP-specific cytoplasmic and nuclear membrane receptor(s), elucidation of their structure-function relationship, and mechanism(s) through which SP-STP breaches cytoplasmic and nuclear membranes/barriers will enhance our understanding on the role of SP-STP in complex mechanisms of GAS pathogenesis.

## REFERENCES


1. Carapetis, J. R., Steer, A. C., Mulholland, E. K., and Weber, M. (2005) The global burden of group A streptococcal diseases. *Lancet Infect. Dis.* **5,** 685–694
2. Olsen R. J., Shelburne, S. A., and Musser, J. M. (2009) Molecular mechanisms underlying group A streptococcal pathogenesis. *Cell. Microbiol.* **11,** 1–12
3. Virtaneva, K., Porcella, S. F., Graham, M. R., Ireland, R. M., Johnson, C. A., Ricklefs, S. M., Babar, I., Parkins, L. D., Romero, R. A., Corn, G. J., Gardner, D. J., Bailey, J. R., Parnell, M. J., and Musser, J. M. (2005) Longitudinal analysis of the group A *Streptococcus transcriptome* in experimental pharyngitis in cynomolgus macaques. *Proc. Natl. Acad. Sci. U.S.A.* **102,** 9014–9019
4. Goldmann, O., Rohde, M., Chhatwal, G. S., and Medina, E. (2004) Role of macrophages in host resistance to group A streptococci. *Infect. Immun.* **72,** 2956–2963
5. Medina, E., Rohde, M., and Chhatwal, G. S. (2003) Intracellular survival of *Streptococcus pyogenes* in polymorphonuclear cells results in increased bacterial virulence. *Infect. Immun.* **71,** 5376–5380
6. Ryan, P. A., Kirk, B. W., Euler, C. W., Schuch, R., and Fischetti, V. A. (2007) Novel algorithms reveal streptococcal transcriptomes and clues about undefined genes. *PLoS Comput. Biol.* **3,** e132
7. Nizet, V. (2007) Understanding how leading bacterial pathogens subvert innate immunity to reveal novel therapeutic targets. *J. Allergy Clin. Immunol.* **120,** 13–22
8. Goldmann, O., Sastalla, I., Wos-Oxley, M., Rohde, M., and Medina, E. (2009) *Streptococcus pyogenes* induces oncosis in macrophages through the activation of an inflammatory programmed cell death pathway. *Cell. Microbiol.* **11,** 138–155
9. Kobayashi, S. D., Braughton, K. R., Whitney, A. R., Voyich, J. M., Schwan, T. G., Musser, J. M., and DeLeo, F. R. (2003) Bacterial pathogens modulate an apoptosis differentiation program in human neutrophils. *Proc. Natl. Acad. Sci. U.S.A.* **100,** 10948–10953
10. Ghosh, J., Caparon, M. G. (2006) Specificity of *Streptococcus pyogenes* $NAD^+$ glycohydrolase in cytolysin-mediated translocation. *Mol. Microbiol.* **62,** 1203–1214
11. Timmer, A. M., Timmer, J. C., Pence, M. A., Hsu, L. C., Ghochani, M., Frey, T. G., Karin, M., Salvesen, G. S., and Nizet, V. (2009) Streptolysin O promotes group A *Streptococcus* immune evasion by accelerated macro-

phage apoptosis. *J. Biol. Chem.* **284,** 862–871
12. Kuo, C. F., Wu, J. J., Tsai, P. J., Kao, F. J., Lei, H. Y., Lin, M. T., and Lin, Y. S. (1999) Streptococcal pyrogenic exotoxin B induces apoptosis and reduces phagocytic activity in U937 cells. *Infect. Immun.* **67,** 126–130
13. Jin, H., Pancholi, V. (2006) Identification and biochemical characterization of a eukaryotic type serine/threonine kinase and its cognate phosphatase in *Streptococcus pyogenes*. Their biological functions and substrate identification. *J. Mol. Biol.* **357,** 1351–1372
14. Agarwal, S., Agarwal, S., Pancholi, P., and Pancholi, V. (2011) Role of serine/threonine phosphatase (SP-STP) in *Streptococcus pyogenes* physiology and virulence. *J. Biol. Chem.* **286,** 41368–41380
15. Shi, Y. (2009) Serine/threonine phosphatases. Mechanism through structure. *Cell* **139,** 468–484
16. Tamura, S., Toriumi, S., Saito, J., Awano, K., Kudo, T. A., and Kobayashi, T. (2006) PP2C family members play key roles in regulation of cell survival and apoptosis. *Cancer Sci.* **97,** 563–567
17. Kansal, R. G., McGeer, A., Low, D. E., Norrby-Teglund, A., and Kotb, M. (2000) Inverse relation between disease severity and expression of the streptococcal cysteine protease, SpeB, among clonal M1T1 isolates recovered from invasive group A streptococcal infection cases. *Infect. Immun.* **68,** 6362–6369
18. Aziz, R. K., and Kotb, M. (2008) Rise and persistence of global M1T1 clone of *Streptococcus pyogenes*. *Emerg. Infect. Dis.* **14,** 1511–1517
19. Pancholi, V., Boël, G., and Jin, H. (2010) *Streptococcus pyogenes* Ser/Thr kinase-regulated cell wall hydrolase is a cell division plane-recognizing and chain-forming virulence factor. *J. Biol. Chem.* **285,** 30861–30874
20. Rainer, J., Sanchez-Cabo, F., Stocker, G., Sturn, A., and Trajanoski, Z. (2006) CARMAweb: comprehensive R- and bioconductor-based web service for microarray data analysis. *Nucleic Acids Res.* **34,** W498–W503
21. Theriot, J. A., Rosenblatt, J., Portnoy, D. A., Goldschmidt-Clermont, P. J., and Mitchison, T. J. (1994) Involvement of profilin in the actin-based motility of *L. monocytogenes* in cells and in cell-free extracts. *Cell* **76,** 505–517
22. Smith, G. A., Portnoy, D. A., and Theriot, J. A. (1995) Asymmetric distribution of the *Listeria monocytogenes* ActA protein is required and sufficient to direct actin-based motility. *Mol. Microbiol.* **17,** 945–951
23. Andrade, M. A., Chacón, P., Merelo, J. J., and Morán, F. (1993) Evaluation of secondary structure of proteins from UV circular dichroism spectra using an unsupervised learning neural network. *Protein Eng.* **6,** 383–390
24. Kreikemeyer, B., McIver, K. S., and Podbielski, A. (2003) Virulence factor regulation and regulatory networks in *Streptococcus pyogenes* and their impact on pathogen-host interactions. *Trends Microbiol.* **11,** 224–232
25. Smoot, L. M., Smoot, J. C., Graham M. R., Somerville, G. A., Sturdevant, D. E., Migliaccio, C. A., Sylva, G. L., and Musser, J. M. (2001) Global differential gene expression in response to growth temperature alteration in group A *Streptococcus*. *Proc. Natl. Acad. Sci. U.S.A.* **98,** 10416–10421
26. Pereira, S. F., Goss, L., and Dworkin, J. (2011) Eukaryote-like serine/threonine kinases and phosphatases in bacteria. *Microbiol. Mol. Biol. Rev.* **75,** 192–212
27. Boël, G., Jin, H., and Pancholi, V. (2005) Inhibition of cell surface export of group A streptococcal anchorless surface dehydrogenase affects bacterial adherence and antiphagocytic properties. *Infect. Immun.* **73,** 6237–6248
28. Jin, H., Agarwal, S., Agarwal, S., and Pancholi, V. (2011) Surface export of GAPDH/SDH, a glycolytic enzyme, is essential for *Streptococcus pyogenes* virulence. *MBio.* **2,** e00068–11
29. Garcia, A., Cayla, X., Guergnon, J., Dessauge, F., Hospital, V., Rebollo, M. P., Fleischer, A., and Rebollo, A. (2003) Serine/threonine protein phosphatases PP1 and PP2A are key players in apoptosis. *Biochimie* **85,** 721–726
30. Rantanen, M. K., Lehtiö, L., Rajagopal, L., Rubens, C. E., and Goldman, A. (2007) Structure of *Streptococcus agalactiae* serine/threonine phosphatase. The subdomain conformation is coupled to the binding of a third metal ion. *FEBS J.* **274,** 3128–3137
31. Hagimoto, N., Kuwano, K., Kawasaki, M., Yoshimi, M., Kaneko, Y., Kunitake, R., Maeyama, T., Tanaka, T., and Hara, N. (1999) Induction of interleukin-8 secretion and apoptosis in bronchiolar epithelial cells by Fas ligation. *Am. J. Respir. Cell Mol. Biol.* **21,** 436–445
32. Wang, Y., Kim, N. S., Haince, J. F., Kang, H. C., David, K. K., Andrabi, S. A., Poirier, G. G., Dawson, V. L., and Dawson, T. M. (2011) Poly(ADP-ribose) (PAR) binding to apoptosis-inducing factor is critical for PAR polymerase-1-dependent cell death (parthanatos). *Sci. Signal.* **4,** ra20
33. Kratzmeier, M., Albig, W., Hanecke, K., and Doenecke, D. (2000) Rapid dephosphorylation of H1 histones after apoptosis induction. *J. Biol. Chem.* **275,** 30478–30486
34. Th'ng, J. P. (2001) Histone modifications and apoptosis: cause or consequence? *Biochem. Cell Biol.* **79,** 305–311
35. Prigent, C., and Dimitrov, S. (2003) Phosphorylation of serine 10 in histone H3, what for? *J. Cell Sci.* **116,** 3677–3685
36. Dong, Z., and Bode, A. M. (2006) The role of histone H3 phosphorylation (Ser-10 and Ser-28) in cell growth and cell transformation. *Mol. Carcinog.* **45,** 416–421
37. Bricker, A. L., Cywes, C., Ashbaugh, C. D., and Wessels, M. R. (2002) $NAD^+$-glycohydrolase acts as an intracellular toxin to enhance the extracellular survival of group A streptococci. *Mol. Microbiol.* **44,** 257–269
38. Tsai, P. J., Lin, Y. S., Kuo, C. F., Lei, H. Y., and Wu, J. J. (1999) Group A *Streptococcus* induces apoptosis in human epithelial cells. *Infect. Immun.* **67,** 4334–4339
39. Nakagawa, I., Nakata, M., Kawabata, S., and Hamada, S. (2001) Cytochrome *c*-mediated caspase-9 activation triggers apoptosis in *Streptococcus pyogenes*-infected epithelial cells. *Cell. Microbiol.* **3,** 395–405
40. Riddle, D. J., Bessen, D. E., and Caparon, M. G. (2010) Variation in *Streptococcus pyogenes* $NAD^+$ glycohydrolase is associated with tissue tropism. *J. Bacteriol.* **192,** 3735–3746
41. Meehl, M. A., Caparon, M. G. (2004) Specificity of streptolysin O in cytolysin-mediated translocation. *Mol. Microbiol.* **52,** 1665–1676
42. Osterlund, A., Popa, R., Nikkilä, T., Scheynius, A., and Engstrand, L. (1997) Intracellular reservoir of *Streptococcus pyogenes in vivo.* A possible explanation for recurrent pharyngotonsillitis. *Laryngoscope* **107,** 640–647
43. Kim, J. Y., Kim, Y. J., Lee, S., and Park, J. H. (2011) BNip3 is a mediator of TNF-induced necrotic cell death. *Apoptosis* **16,** 114–126
44. Sprick, M. R., Rieser, E., Stahl, H., Grosse-Wilde, A., Weigand, M. A., and Walczak, H. (2002) Caspase-10 is recruited to and activated at the native TRAIL and CD95 death-inducing signaling complexes in a FADD-dependent manner but can not functionally substitute caspase-8. *EMBO J.* **21,** 4520–4530
45. Afford, S. C., Randhawa, S., Eliopoulos, A. G., Hubscher, S. G., Young, L. S., and Adams, D. H. (1999) CD40 activation induces apoptosis in cultured human hepatocytes via induction of cell surface fas ligand expression and amplifies fas-mediated hepatocyte death during allograft rejection. *J. Exp. Med.* **189,** 441–446
46. Tong, Y., Yang, Q., Vater, C., Venkatesh, L. K., Custeau, D., Chittenden, T., Chinnadurai, G., and Gourdeau, H. (2001) The pro-apoptotic protein, Bik, exhibits potent antitumor activity that is dependent on its BH3 domain. *Mol. Cancer Ther.* **1,** 95–102
47. Cardone, M. H., Roy, N., Stennicke, H. R., Salvesen, G. S., Franke, T. F., Stanbridge, E., Frisch, S., and Reed, J. C. (1998) Regulation of cell death protease caspase-9 by phosphorylation. *Science* **282,** 1318–1321
48. Sinha, D., Bannergee, S., Schwartz, J. H., Lieberthal, W., and Levine, J. S. (2004) Inhibition of ligand-independent ERK1/2 activity in kidney proximal tubular cells deprived of soluble survival factors up-regulates Akt and prevents apoptosis. *J. Biol. Chem.* **279,** 10962–10972
49. Kobayashi, S., Kajino, S., Takahashi, N., Kanazawa, S., Imai, K., Hibi, Y., Ohara, H., Itoh, M., and Okamoto, T. (2005) 53BP2 induces apoptosis through the mitochondrial death pathway. *Genes Cells* **10,** 253–260
50. North, J. A., Javaid, S., Ferdinand, M. B., Chatterjee, N., Picking, J. W., Shoffner, M., Nakkula, R. J., Bartholomew, B., Ottesen, J. J., Fishel, R., and Poirier, M. G. (2011) Phosphorylation of histone H3 (T118) alters nucleosome dynamics and remodeling. *Nucleic Acids Res.* **39,** 6465–6474
51. Bode, A. M., and Dong, Z. (2005) Inducible covalent post-translational modification of histone H3. *Sci. STKE 2005,* re4
52. Jeon, E. S., Lee, M. J., Sung, S. M., and Kim, J. H. (2007) Sphingosylphosphorylcholine induces apoptosis of endothelial cells through reactive oxygen species-mediated activation of ERK. *J. Cell. Biochem.* **100,** 1536–1547